53p

NASA TN D-1639

TECHNICAL NOTE

D-1639

ORBITAL ERROR ANALYSIS OF THE SCOUT RESEARCH VEHICLE

By C. H. Woodling, Jarrell R. Elliott, and Paul J. Stull

Langley Research Center
Langley Station, Hampton, Va.

NATIONAL AERONAUTICS AND SPACE ADMINISTRATION
WASHINGTON
May 1963

Code-1

NATIONAL AERONAUTICS AND SPACE ADMINISTRATION

TECHNICAL NOTE D-1639

ORBITAL ERROR ANALYSIS OF THE SCOUT RESEARCH VEHICLE

By C. H. Woodling, Jarrell R. Elliott, and Paul J. Stull

SUMMARY

A statistical error analysis has been made of the orbital-accuracy capability of the Scout research vehicle. Twenty-six independent error sources were included in the analysis. Orbital-altitude error bands were determined for three nominal circular orbits at altitudes of 120, 300, and 600 nautical miles. In addition, for the 300-nautical-mile mission, a detailed examination was made of the effects of the separate errors; predominant error sources were determined and an analysis was made of the effect on the orbital accuracy of injecting into the orbit with a velocity greater than that for circular. Also a method for determining an enclosed area in apogee-perigee space (within which approximately 95 percent of all orbits will occur) is described and applied to the 300-nautical-mile mission.

The results from this analysis indicate that the 95-percent-probability or 2σ error bands for the 120-, 300-, and 600-nautical-mile nominal circular orbits have maximum variations from the nominal altitudes of approximately ± 100, ± 110, and ± 150 nautical miles, respectively. It was found that these error bands are critically dependent upon the fourth-stage tip-off error and will be appreciably less if the present fourth-stage separation system can be shown to have a 2σ value for tip-off of less than the 3.5° assumed in this analysis. For example, for the 300-nautical-mile mission, the maximum uncertainty in orbital altitude of a 95-percent basis is reduced to ± 85 nautical miles for a 2σ value of tip-off of about 2°. The results also indicate that the overall orbital accuracy of the Scout vehicle cannot be significantly improved, exclusive of tip-off, until the rocket parameters (specific impulse, propellant weight, and propellant burning rate) can be defined to within smaller variations than those assumed for this analysis. The effect of injecting into the orbit with a velocity greater than that for circular was found to reduce considerably the uncertainties about the minimum orbital altitude (the perigee of the orbit).

INTRODUCTION

The Scout research vehicle is a four-stage solid-fuel rocket system designed to give the National Aeronautics and Space Administration an economical, reliable, and versatile vehicle capable of both probe and orbital missions. Guidance of the Scout vehicle is achieved by a three-axis "strapped down" gyro system in combination with a three-axis control system. Control of the vehicle flight path

is obtained indirectly by preprograming zero yaw and roll rates and a pitch-rate command such that essentially a gravity-turn trajectory is executed. While this method of guidance is simple and relatively inexpensive compared with inertial systems or those employing a ground loop, the accuracy of such a system is critically dependent on the ability to predict the total system performance and operation of the vehicle. The purpose of this paper is to examine the possible factors and/or variables affecting the Scout guidance accuracy and to determine by statistical methods the combined effect of these factors on the Scout orbital-accuracy capability.

The statistical methods employed were to consider each factor as an independent, normally distributed error source, to assume a specified value of the standard deviation of the error in each of the factors, and to insert each of these values in turn into the appropriate equations to determine the altitude variation during one orbit from an orbit calculation containing no errors. The individual altitude variations were then summed statistically to determine the total statistical orbit-altitude variation.

SYMBOLS

a speed of sound, ft/sec

A_e exit area of rocket motor, sq ft

b thrust offset distance, ft

C_A axial-force coefficient

C_m pitching-moment coefficient

$C_{m_\delta} = \frac{\partial C_m}{\partial \delta}$, per radian

$C_{m_q} = \frac{\partial C_m}{\partial\left(\frac{\dot{\theta} d}{2V_a}\right)}$, per radian

C_N normal-force coefficient

$C_{N_\delta} = \frac{\partial C_N}{\partial \delta}$, per radian

d reference length, ft

F force, lb

F_{a_X}, F_{a_Z}	aerodynamic forces along X- and Z-body axis, lb
F_{c_Z}	control force along Z-body axis, lb
F_{T_X}, F_{T_Z}	thrust forces along X- and Z-body axis, lb
F_{δ_v}	control force due to jet vanes, lb/radian
F_X, F_Z	total forces along X- and Z-body axis, lb
h	altitude above surface of earth, ft (unless otherwise specified)
h_a	apogee altitude of orbit, ft
h_p	perigee altitude of orbit, ft
i	orbit inclination, deg
I_{sp}	specific impulse, lb-sec/lb
I_t	total impulse, lb-sec
I_Y	moment of inertia about Y-body axis, slug-ft^2
j	integer
K_θ	control-system position gain, radian/radian
$K_{\dot{\theta}}$	control-system rate gain, radian/radian/sec
L	latitude, radian
M	Mach number
M_Y	moment about Y-body axis, ft-lb
M_{a_Y}	pitching moment about the Y-body axis due to aerodynamic forces, ft-lb
M_{T_Y}	pitching moment about the Y-body axis due to thrust misalinement, ft-lb
m	mass, slugs
n	number
P	atmospheric pressure, lb/ft^2

q	angular velocity about the Y-body axis, radians/sec
$\bar{q}$	dynamic pressure, lb/ft^2
r	distance from vehicle to center of earth, ft
R	earth radius, ft
S	reference area, ft^2
T	sea-level thrust, lb
T'	altitude thrust, lb
T_j	control-jet thrust, lb
t	time
V	inertial velocity, ft/sec
V_a	aerodynamic velocity, ft/sec
V_c	circular orbit velocity, ft/sec
V_i	injection velocity, ft/sec
V_w	wind velocity, ft/sec (headwind is positive)
W	weight, lb
W_p	propellant weight, lb
$\dot{W}_p$	propellant flow rate, lb/sec
x_{cg}	center of gravity along X-body axis, ft
x_{cg_o}	reference center of gravity along X-body axis, ft
x_j	body-station location of control jet on X-body axis
x_v	distance along X-body axis from jet vanes to x_{cg_o}, ft
α	inertial angle of attack, radians
α_a	aerodynamic angle of attack, radians
γ	inertial flight-path angle, radians

γ_a aerodynamic flight-path angle, radians

Δ_c control dead band, radians

δ control-surface deflection, radians

ϵ control-error signal, radians

θ pitch angle, radians

θ_o initial pitch angle, radians

θ_c commanded pitch angle, radians

λ longitude, radians

ρ density, slug/ft^3

σ standard deviation $\left(\text{root mean square of the deviations, } x_i, \text{ of a set of observations from the true value, i.e., } \sigma = \sqrt{\frac{\sum_{i=1}^{n} x_i^2}{n}}\right)$

τ thrust-misalinement angle, radians

ϕ range angle, radians

ψ inertial azimuth angle, radians

ω earth rotational rate, radians/sec

Subscripts:

b web burnout time

BO burnout

nom nominal

t total

A Δ prefix to a quantity indicates a variation from some nominal condition.

A dot over a variable indicates differentiation with respect to time.

SCOUT LAUNCH PROCEDURE

Prior to describing the methods of analysis and examining the various parameters that were considered in assessing the Scout accuracy, it is helpful first to describe briefly a typical launch trajectory for an orbital mission. For launches from Wallops Island, Virginia, the vehicle is launched from a tower (fig. 1) at an elevation angle between 78° and 88°. The tower is mounted on tracks to provide a choice in launch azimuth. From lift-off the vehicle pitch attitude is controlled to follow a preprogramed attitude which will, for nominal vehicle performance and in the absence of disturbances, produce a gravity-turn (ballistic) trajectory. The vehicle orientation in roll and azimuth during the ascent is maintained at the initial launch-reference attitude. A proportional servocontrol system which operates aerodynamic tip surfaces augmented by jet vanes during first-stage burning is used to control the vehicle during the first-stage phase of flight. After first-stage burnout the complete vehicle is allowed to coast to an altitude of 130,000 feet. The second stage is then ignited and a diaphragm separation system blast separates it from the first stage. Control during both second- and third-stage flight is provided by hydrogen peroxide reaction jets operating as an on-off system. Following second-stage burnout, the vehicle coasts for a short period after which the third-stage motor is ignited, and is separated from the second stage by a diaphragm separation system. After third-stage burnout the vehicle with its hydrogen peroxide control system still operating coasts to the apogee of the ascent trajectory. At this time the fourth stage, having been alined during coast to the proper attitude by the third-stage control system, is spun up for spin stabilization. In the early development of the Scout vehicle and for the first seven flights the diaphragm system was used for fourth-stage separation because of its inherent simplicity and positive separation after ignition. However, the flight-test data indicated severe fourth-stage tip-off disturbances which were subsequently traced to the diaphragm system. Consequently, later development vehicles have incorporated a spring separation mechanism which insures positive separation by pulling away of the third stage by using the third-stage pitch- and yaw-control jets as the power source. Several early test flights have indicated a sizable reduction

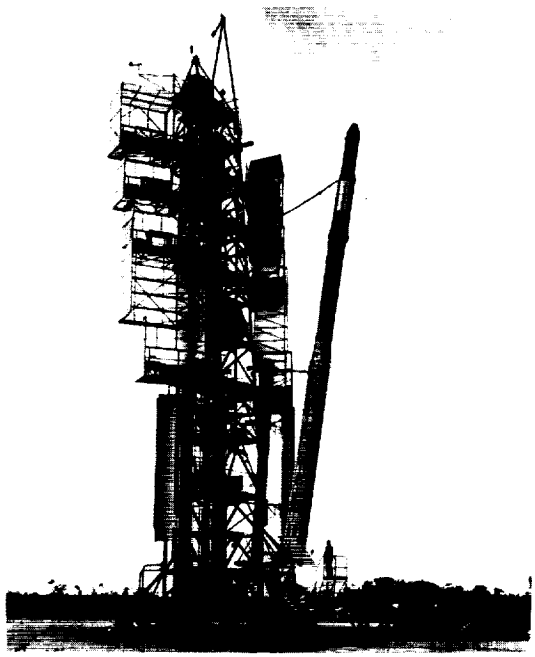

L-61-3853

Figure 1.- Scout vehicle on launch tower.

in separation disturbances. A typical four-stage nominal ascent trajectory is illustrated in figure 2.

METHODS OF COMPUTATION AND ANALYSIS

Launch Trajectory

The launch trajectories were calculated by using the equations of motion presented in appendix A. These are two-dimensional (single plane) equations which include the vehicle angular degree of freedom in pitch. The calculations assumed a spherical, rotating earth. All launches were made due east from Wallops Island, Virginia, with a launch latitude of 37.85° north and longitude of 75.47° west. Since the equations of motion do not include the degree of freedom in roll, for the fourth-stage portion of the trajectory where the stage is spinning, perfect stabilization was assumed and simulated in the computer calculations by holding an inertially fixed pitch attitude.

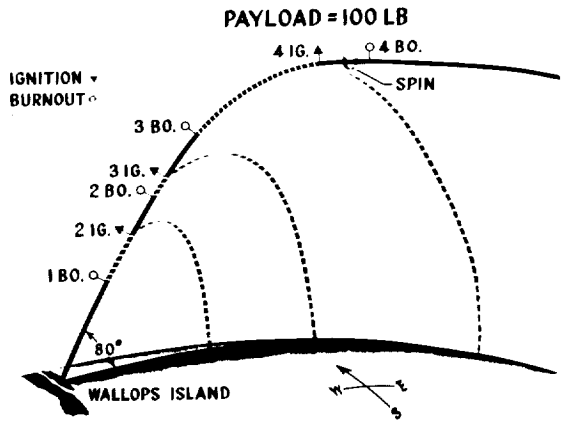

Figure 2.- Scout orbital-ascent trajectory.

A suitable launch trajectory was established to produce each nominal orbit by adjusting the payload weight and launch elevation angle. Each of 26 error sources was then introduced one at a time, and the basic launch trajectory was rerun (stage ignition times and the pitch program were held fixed). Actually two launch trajectories were calculated for each error source by including both a plus and a minus value of the error, thus resulting in 52 error cases for each nominal orbit. It should be mentioned that in order to minimize the digital-computing inaccuracies involved with small differences, the actual value of the errors used in computing the trajectories were the 3σ values. Table I presents a list of the 26 error sources considered. The 2σ data presented were obtained by taking two-thirds of the error values used in the trajectory calculations. The 95-percent probability associated with 2σ values was considered to be the probability range of most general interest.

Orbital-Altitude Variation

For each set of injection conditions, the associated orbit was calculated and the orbital altitude at equal increments of earth range angle from 0° to 360° was tabulated. A plot of results such as these is shown in figure 3. Here orbital altitude is plotted against the range angle ϕ, where $\phi = 0°$ is the point of injection. The two typical orbits plotted show the two orbits resulting from $\pm 2\sigma$ values of one error source. A nominal circular orbit is also shown as

a straight line. As the final step, differences in orbital altitude Δh from the nominal altitude at the discrete values of range angle were determined. The

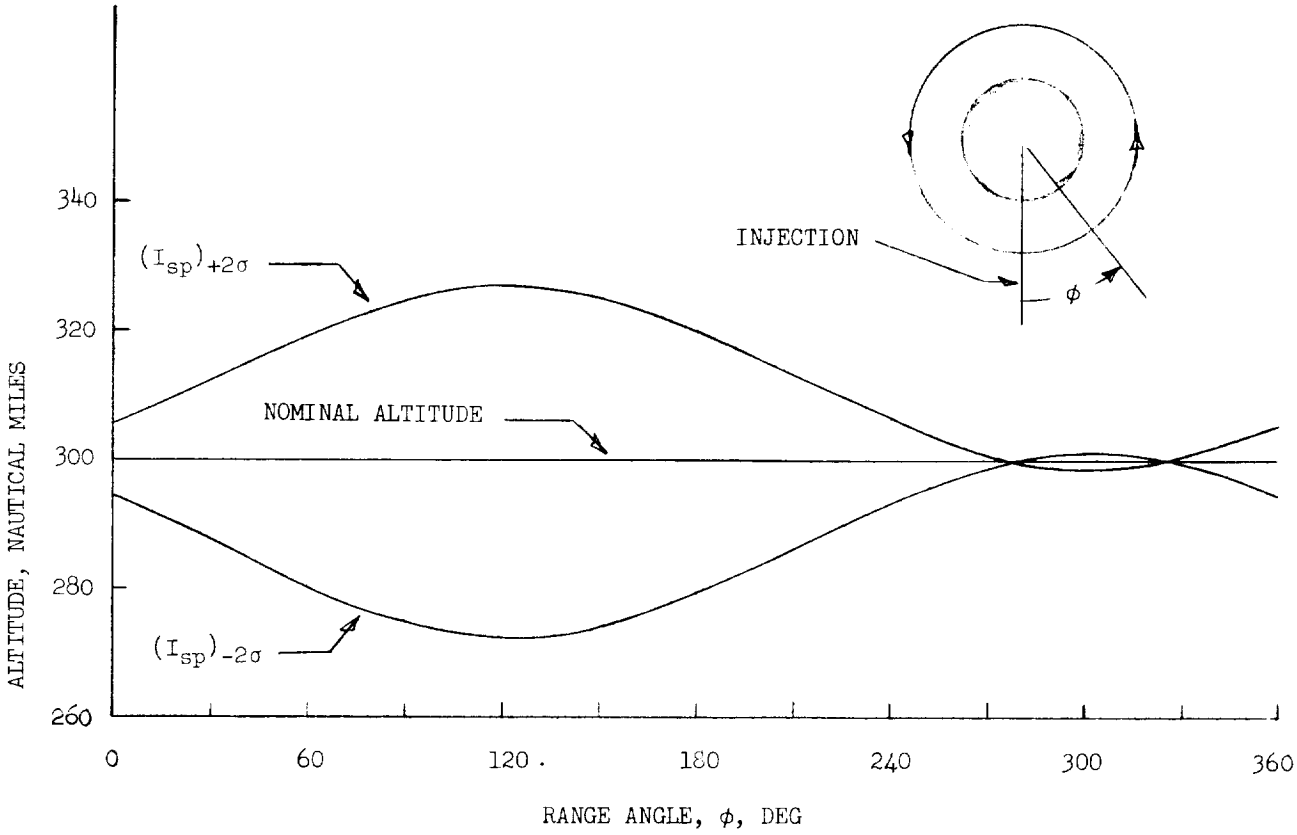

Figure 3.- Orbital altitude for a nominal circular orbit of 300 nautical miles and $\pm 2\sigma$ variation of first stage I_{sp}.

values of Δh were determined in this manner for all 52 orbits. It should be mentioned that the range angle traversed during the ascent (from launch to the point of injection) actually varied slightly from the nominal case as might be expected. This variation, however, was quite small for the individual cases (0.1° maximum) and hence the method described for determining the values of Δh at like values of range angle is considered valid.

Statistical Combination

To obtain the total statistical variation (2σ) in orbital altitude for a given nominal orbit, that is, to combine the effect of all the errors, the values of Δh of all the cases at like range angles were root-summed square (RSS), that is, the total 2σ altitude was

$$(\Delta h)_{2\sigma} = \sqrt{\sum_{i=1}^{26} \left(\Delta h_i\right)^2} \qquad (1)$$

In particular, two totals were obtained at each range angle - the RSS value of the positive values of Δh and the RSS value of the negative values of Δh. The RSS value of the positive Δh's was then used as the increase from the nominal altitude and denoted as $(\Delta h)_{+2\sigma}$ and the RSS value of the negative Δh's was used as the decrease from the nominal altitude and denoted as $(\Delta h)_{-2\sigma}$. Although this treatment of the positive and negative variations separately does not have any mathematical basis in statistics, the approach appears reasonable from an engineering point of view. The difference in $(\Delta h)_{+2\sigma}$ and $(\Delta h)_{-2\sigma}$ is due to the nonlinearity of the equations of motion for the perturbed trajectory. These RSS equations, however, are completely valid only in the case of linear equations of perturbed motion. It was assumed that the statistical treatment of the $(\Delta h)_{+2\sigma}$ and the $(\Delta h)_{-2\sigma}$ output of these somewhat nonlinear equations by use of a linear analysis was justified for purposes of engineering accuracy. This is particularly true in view of the uncertainty in the standard deviations assumed for the error-source inputs. In a few instances it was found in the summing process that the plus and minus 2σ value of the same error source resulted in Δh values of like signs at certain range angles. In such instances only the larger of the two Δh values was considered, thus effectively using a zero error for the Δh of opposite sign. Finally, a plot of the RSS values of altitude against range angle yields an altitude band about the nominal orbit such as shown in figure 4. In this figure at each discrete range angle the $(\Delta h)_{+2\sigma}$ value was added to the nominal orbit altitude and the $(\Delta h)_{-2\sigma}$ value was subtracted to obtain the altitude band shown. Statistically this plot is interpreted as the altitude band about the nominal orbit within which 95 percent of all the orbits will occur. If the intended mission is a 300-nautical-mile circular orbit then the actual orbit will have a 95-percent probability of falling within the boundaries shown.

In order to obtain statistical information on the pairing of apogee and perigee altitudes for any orbit, a Monte Carlo analysis (described in appendix B) was performed on the injection conditions obtained from the ascent trajectory equations. As an adjunct to this analysis, it was considered informative to examine the statistical variation of Δh at various range angles. This examination, at least within the limitations of the analysis, shows the variation of Δh to be Gaussian. A discussion of this is found in appendix B. The 2σ value of Δh from this analysis is compared in figure 4 with the 2σ results of the RSS analysis. Good agreement is noted.

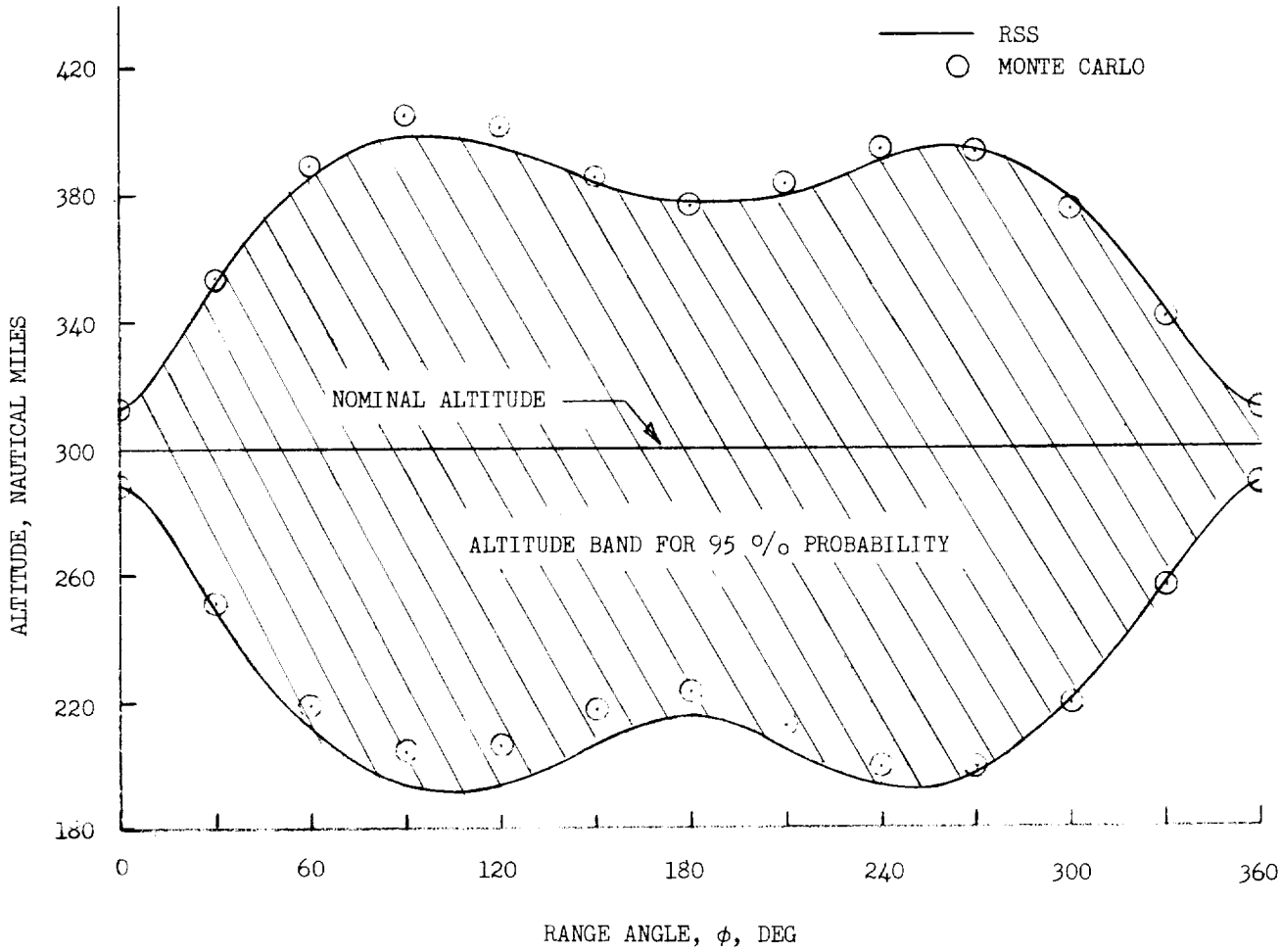

Figure 4.- The 2σ altitude band for a nominal circular orbit of 300 nautical miles.

ERROR SOURCES AND MAGNITUDES

The error sources included in the analysis and the 2σ variations used for the respective parameters are listed in table I. For the purpose of this analysis it was assumed that these parameters are normally distributed about their expected or nominal value. Furthermore, necessary to the analysis is the basic assumption that these error sources are completely independent. It must be mentioned that because of the limited number of accurate samples available for most of these parameters, the magnitudes of the standard deviations used were mainly educated guesses. For the rocket parameters, which are shown in the section entitled "Results and Discussion" to be the dominating error parameters, an attempt has been made to compare the 2σ values listed in table I with data for the Scout rockets obtained from flight and some ground firings. These data are included in appendix C along with a comparison of some of the results of this analysis with flight measured quantities.

Specific Impulse, Propellant Flow Rate, and Propellant Weight

These three error sources are variables associated with the solid-rocket motors. Although in the practical case it may be argued that these three are not entirely independent, they were handled independently in the analysis and were so chosen from the following considerations. Consider the instantaneous thrust to be

$$T = I_{sp}\dot{W}_p \tag{2}$$

then for I_{sp} constant,

$$I_t = \int_0^{t_{BO}} T\,dt = I_{sp}\int_0^{t_{BO}} \dot{W}_p\,dt \tag{3}$$

and also

$$\int_0^{t_{BO}} \dot{W}_p\,dt = W_p \tag{4}$$

Now it is reasonable to assume that uncertainties will exist in the values for I_{sp} and $\dot{W}_p$, and from equation (2) such uncertainties will result in variations of the thrust from the expected value. In addition, uncertainties might also be expected in the total propellant weight on board. The actual procedure followed then in the simulation was to vary one of the three while the other two were held at their nominal values. Specifically this was accomplished as follows: As shown in appendix A, thrust was included in the digital program as a tabular function of time and propellant flow rate was generated as

$$\dot{W}_p = -\frac{T}{I_{sp}} \tag{5}$$

Hence for error 1, I_{sp} was varied, and $\dot{W}_p$ and W_p remained at their nominal value, then in accord with equation (5), thrust was increased or decreased by the same factor as I_{sp} so that $\dot{W}_p$ remained nominal. Burnout time t_{BO} was kept nominal so that W_p remained at its nominal value (eq. (4)). Notice for this case that the variation in total impulse (eqs. (2) and (3)) is equal to the variation in specific impulse. An example of the resulting thrust-time plots included in the machine setup is shown in figure 5(a) for the first-stage motor. The 2σ value assumed for I_{sp} was 1.0 percent for stages 1, 2, and 3 and 0.35 percent for stage 4.

For error 2, $\dot{W}_p$ was varied, I_{sp} and W_p were nominal, and in order to satisfy equation (5), thrust was changed (I_{sp} was nominal) to produce the desired variation of $\dot{W}_p$. Then t_{BO} was adjusted such that W_p remained at

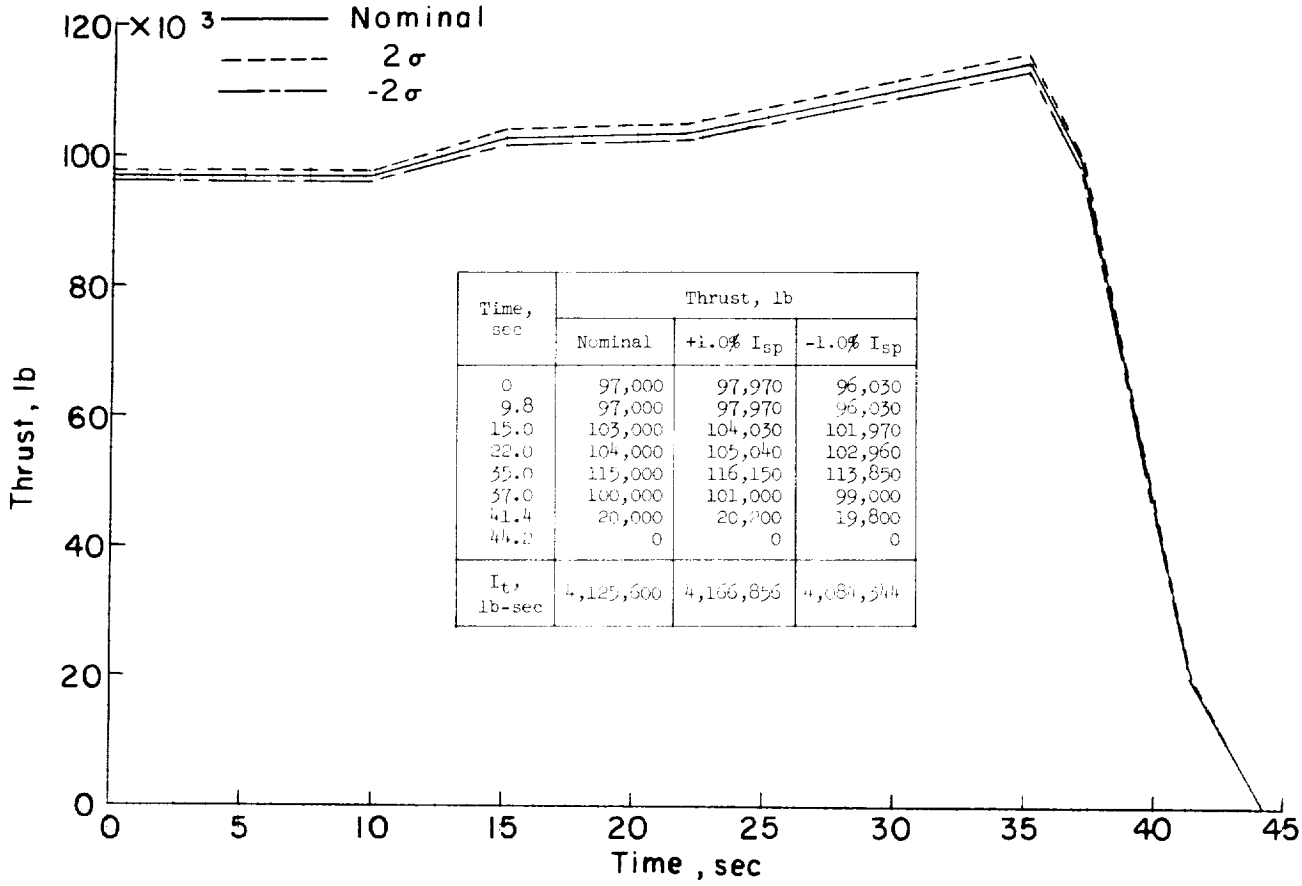

Time, sec	Thrust, lb		
	Nominal	+1.0% I_{sp}	-1.0% I_{sp}
0	97,000	97,970	96,030
9.8	97,000	97,970	96,030
15.0	103,000	104,030	101,970
22.0	104,000	105,040	102,960
35.0	115,000	116,150	113,850
37.0	100,000	101,000	99,000
41.4	20,000	20,200	19,800
44.2	0	0	0
I_t, lb-sec	4,125,600	4,166,856	4,084,344

(a) I_{sp}, varied; $\dot{W}_p$ and W_p nominal.

Figure 5.- First-stage thrust-time plots used in the analysis to simulate rocket parameter variations.

its nominal value. Notice for this variation that since W_p and I_{sp} remain unchanged, from equations (2) and (3) the total impulse remains unchanged. An example of the resulting thrust-time plots included in the machine setup for the $\dot{W}_p$ variation is shown in figure 5(b) for the first-stage motor. It should be noted that the thrust variations relative to the nominal during thrust tail-off are not consistent with the variations before tail-off. This was necessary in order to maintain the same general thrust tail-off characteristics exhibited by the nominal thrust-time plot. A 2σ value of 3.3 percent was used for all four rocket motors. Although some differences have been noticed between the predicted burning times and flight measured times for various motors (see appendix C) the exact variation in burning rate is difficult to determine.

For error 3 I_{sp} and $\dot{W}_p$ were nominal and W_p was varied by the desired amount with the stage full weight being changed accordingly. Burnout time was

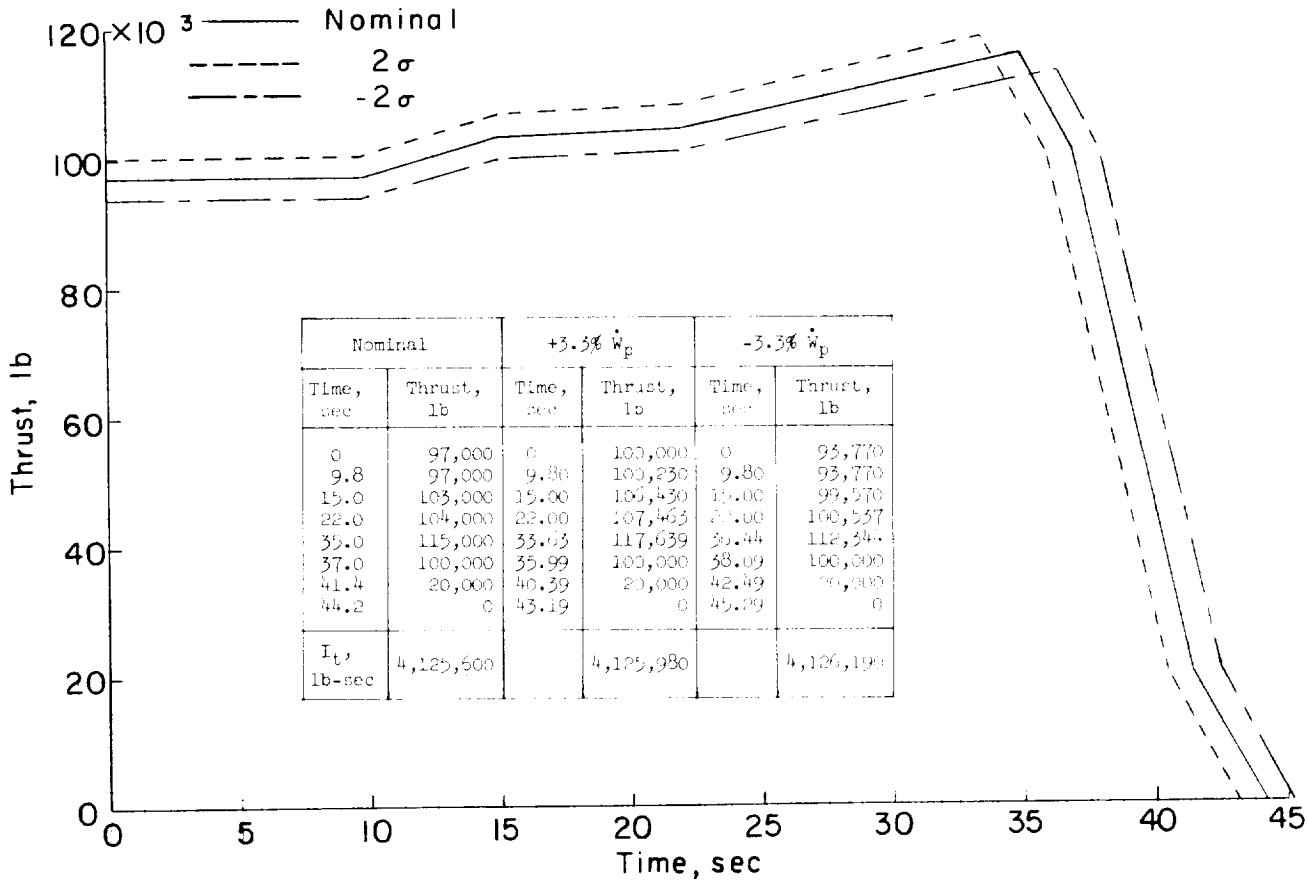

Nominal		+3.3% $\dot{W}_p$		-3.3% $\dot{W}_p$	
Time, sec	Thrust, lb	Time, sec	Thrust, lb	Time, sec	Thrust, lb
0	97,000	0	100,000	0	93,770
9.8	97,000	9.80	100,230	9.80	93,770
15.0	103,000	15.00	106,430	15.00	99,570
22.0	104,000	22.00	107,463	22.00	100,537
33.0	115,000	33.03	117,639	32.44	112,346
37.0	100,000	35.99	100,000	38.09	100,000
41.4	20,000	40.39	20,000	42.49	20,000
44.2	0	43.19	0	45.29	0
I_t, lb-sec	4,125,600		4,135,980		4,126,190

(b) $\dot{W}_p$ varied; I_{sp} and W_p nominal.

Figure 5.- Continued.

adjusted such that the integral $\int_0^{t_{BO}} \dot{W}_p \, dt$ was equal to the new value of W_p. Notice that this results in a change in total impulse (eq. (3)) equal to the variation in W_p. Typical thrust-time plots are presented in figure 5(c) for the first-stage motor. Notice here again from the figure that the tail-off characteristics were adjusted in a particular way in order to maintain the same general thrust tail-off characteristics. The assumed 2σ variation of 0.67 percent might appear to be fairly large in that careful weighing of a specific motor empty and full should determine the propellant weight to better accuracy. Although this is probably true in most cases (particularly for the smaller upper stages), the variation of 0.67 percent is taken to include materials in the motor, not actual propellant grain that unintentionally burn or, on the other hand, propellant itself that is left unburned.

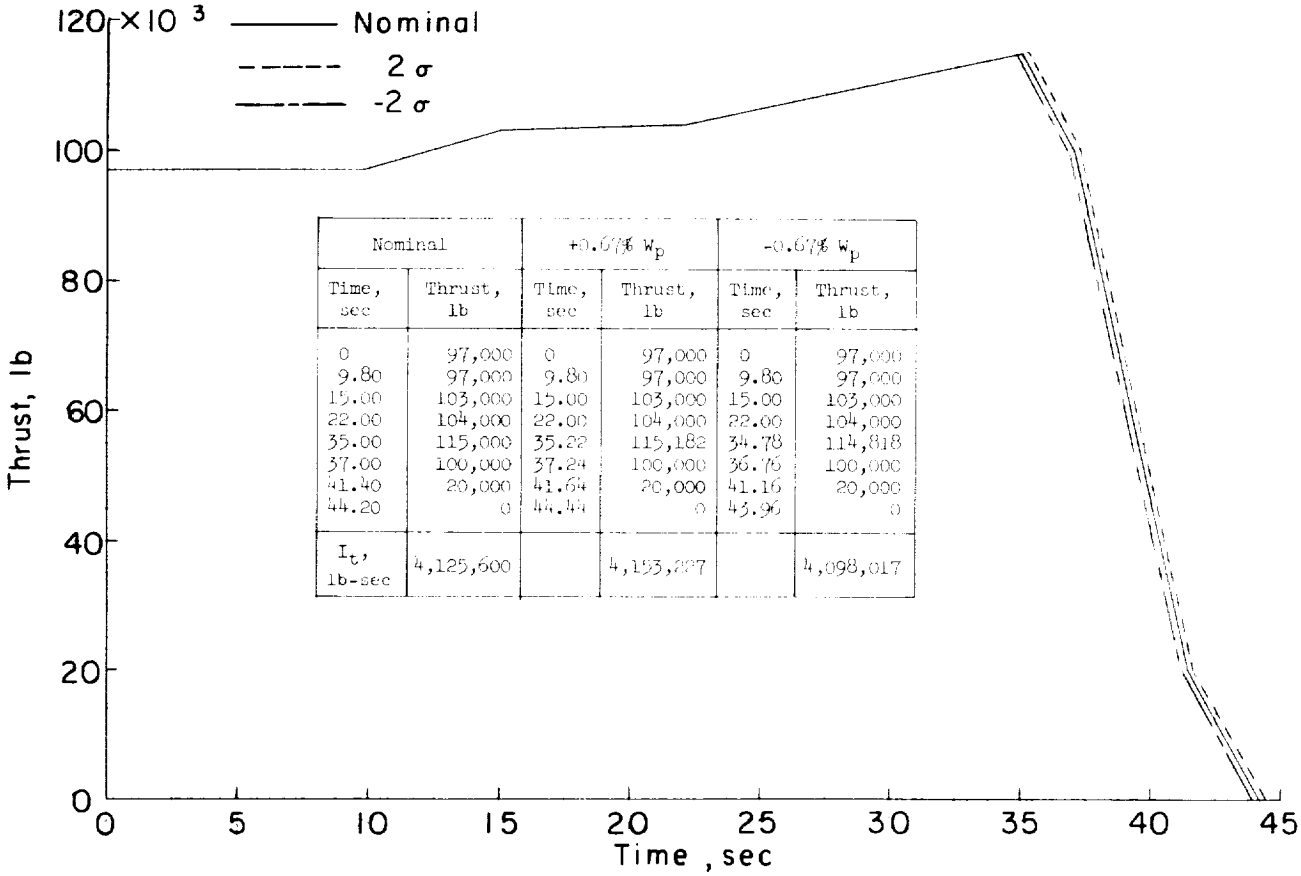

Nominal		+0.67% W_p		-0.67% W_p	
Time, sec	Thrust, lb	Time, sec	Thrust, lb	Time, sec	Thrust, lb
0	97,000	0	97,000	0	97,000
9.80	97,000	9.80	97,000	9.80	97,000
15.00	103,000	15.00	103,000	15.00	103,000
22.00	104,000	22.00	104,000	22.00	104,000
35.00	115,000	35.22	115,182	34.78	114,818
37.00	100,000	37.24	100,000	36.76	100,000
41.40	20,000	41.64	20,000	41.16	20,000
44.20	0	44.44	0	43.96	0
I_t, lb-sec	4,125,600		4,153,227		4,098,017

(c) W_p varied; I_{sp} and $\dot{W}_p$ nominal.

Figure 5.- Concluded.

Launch Attitude

The effect of an error in the launch attitude was included by assuming an error in θ_o while keeping the commanded attitude θ_c at the nominal value. This simulates the condition where the commanded pitch attitude is correct, but the vehicle comes off the launcher with an error in the pitch angle. The optical methods of prelaunch alinement employed are extremely accurate and actually allow a much better tolerance in launch attitude than the 2σ value assumed. However, the 0.33° value was used to include possible errors in launch attitude that might occur immediately after launch as a result of vehicle motion induced by gusts, "seeking" of the correct attitude, and other unknowns.

Attitude Program

An error in the pitch attitude command was assumed by introducing a shift or bias of 0.13° in the commanded attitude-time curve θ_c. To properly simulate this error, the initial launch attitude θ_o was assumed to be equal to the incorrect θ_c at launch. In other words, if an error existed in programed attitude at launch, the optical alinement would be made to the improper attitude and the vehicle would be launched with an error in attitude.

Thrust Misalinement

If the thrust vector is not directed through the vehicle center of gravity, a moment results which will tend to produce a deviation in the missile attitude from the nominal value. Reasons for misalinement of the thrust include static misalinement of the nozzle with the motor, mass asymmetries (c.g. not on the vehicle center line or thrust line), and physical changes of the nozzle during burning. The measure used here to indicate the magnitude of thrust misalinement is the angle between the thrust vector and the body longitudinal axis. The standard deviation values assumed were based on the vehicle design tolerance for thrust misalinement. The design values of thrust-misalinement angle for the first-, second-, and third-stage motors were 0.25°, 0.20°, and 0.10°, respectively. These then were taken as the three standard deviation values and the two standard values indicated in table I are two-thirds of these numbers. It should be pointed out that this discussion treats only the possible variation in thrust-misalinement magnitude but not in direction. In actuality the thrust vector may be oriented anywhere within the 360° arc around the desired direction. Since this analysis considered only the error sources in the vehicle pitch plane, the standard variation values used should probably be reduced to account for the possible occurrence of the thrust vector out of this plane. This was not done, however, since the magnitude of the standard deviation for the thrust-misalinement angle was an estimated value in the first place. As mentioned in the section entitled "Methods of Computation and Analysis" the digital setup did not compute the trajectory for the fourth stage actually spinning so that thrust misalinement as such could not be considered for the fourth stage. However, the effect of a thrust misalinement on the fourth stage would be to cause an attitude error and this error was included as a part of another error source (see section entitled "Tip-off").

Winds

Standard operation in the preflight trajectory planning and pitch-command determination for a given Scout flight has been to assume zero winds. In flight, however, the presence of winds will cause variations from the intended or nominal trajectory. The 2σ wind profile is shown in figure 6. This is a composite of wind profiles from many sources. This profile was included in the calculations both as a local horizontal headwind and tailwind but only in the first-stage portion of the trajectory. Some thought has been given to the inclusion of some mean or average wind in the preflight trajectory planning for future shots, and if this is done, this particular error effect would have to be reevaluated.

Tip-Off

Tip-off disturbances or disturbances due to separation effects, which result in angular variations from the intended vehicle attitude may occur during the various stage separations. In the case of the separation of the first and second and also the second and third, such disturbances are quickly corrected by the control system and therefore are assumed negligible in this study. However, since the fourth stage is spin stabilized these separation disturbances produce vehicle-attitude errors which will remain uncorrected and therefore must be considered. The fourth stage may also experience attitude deviations due to factors other than separation disturbance, such as thrust misalinement, spin-rocket misalinement, and principal axis asymmetry.

As a result of large altitude errors of the fourth stage exhibited in flights of the early vehicles (see ref. 1), the original separation system and procedures have been modified as mentioned previously. Flights with the new separation system have indicated greatly reduced attitude deviations during fourth-stage separation and burning compared with the deviations apparent in the earlier flights. A 2σ value of 3.5° was used throughout this study. However, in light of the flight results using the new separation system, this value would appear to be high. Adjustment of the results to include a smaller 2σ value is easily done and will be discussed in the section entitled "Results and Discussion."

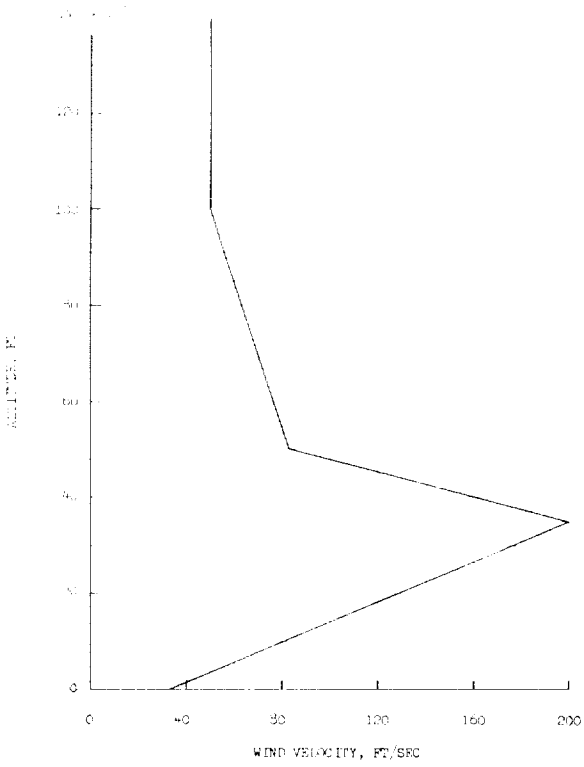

Figure 6.- The 2σ wind profile used in the error analysis.

Dead Band

Prior to fourth-stage ignition and separation from the third stage, the third-stage reaction control system is operating to hold the vehicle at the programed attitude. The pitch attitude of the vehicle during this time is actually oscillating about the programed attitude between the control dead-band limits. At ignition, therefore, the spinning fourth stage may assume an attitude which is in error from the programed attitude by a value dependent on the dead-band magnitude. The dead-band value in the pitch plane prior to fourth-stage ignition is $\pm 0.23^{\circ}$. A 2σ value of $\pm 0.15^{\circ}$ was assumed.

Drag Coefficient

The vehicle aerodynamic characteristics that are necessary in the preflight planning and trajectory prediction have been obtained through wind-tunnel testing

and theoretical calculations. Total configuration drag appears as one of the most important aerodynamic characteristics in that variations in drag from the predicted value will directly affect the calculated vehicle performance. Drag characteristics are modified for each specific flight vehicle according to the payload size and shape, number of antennas, and so forth. Still, uncertainties must be assumed for such things as the effect of Reynolds number on the wind-tunnel data, modification of existing data to account for configuration changes, and different surface roughness for different vehicles. For the total vehicle configuration a 2σ variation of 6.7 percent was assumed for the curve of the basic drag coefficient against Mach number. No variation in the drag characteristics was considered for the second-stage portion of the trajectory.

Static Margin

As in the case of drag, pitching-moment characteristics were obtained for a number of different Scout nose cones and payload configurations. However, in some instances the flight configuration will vary from the tested configurations and will then require theoretical modifications of the tunnel data. To account for uncertainties in the pitching-moment characteristics of the flight vehicle, a 2σ variation in the pitching-moment curve as produced by a static-margin variation of one body diameter (40 inches) was assumed.

Stage Dry Weight

The overall or total weight of a flight vehicle is determined by weighing the separate parts (usually weighed by stage). Dry weight of a stage as used here refers to the total stage weight less the propellant weight W_p. Since uncertainties in W_p are being considered as a separate variation, stage dry weight uncertainties would have to be assumed to arise primarily from the accuracy of weighing a given stage. A 2σ variation of 0.33 percent of the stage dry weight was assumed for each stage.

RESULTS AND DISCUSSION

Orbital-altitude error bands have been determined for the Scout for three nominal circular orbits at altitudes of 120, 300, and 600 nautical miles. In addition, for the 300-nautical-mile mission, a detailed examination has been made of the effects of the separate errors; predominant error sources have been determined and an analysis has been made of the effect on the orbital accuracy of injecting into the orbit with a velocity greater than circular.

The results presented with the associated figures and tables are summarized as follows:

Data	Figure or table
1. Orbital-altitude error bands for nominal circular orbits for altitudes of 120, 300, and 600 nautical miles.	Figure 7
2. The 2σ values of ΔV, Δh, and $\Delta\gamma$ at injection for nominal circular orbits of 120, 300, and 600 nautical miles.	Table II
3. Variations of ΔV, Δh, and $\Delta\gamma$ due to each error source at second-, third-, and fourth-stage ignition for 300-nautical-mile nominal orbit.	Table III
4. Variations of ΔV, Δh, and $\Delta\gamma$ at injection and orbital-altitude variation Δh at range-angle increments due to each error source for 300-nautical-mile nominal orbit.	Table IV
5. Predominant error sources including the effect of the rocket parameters and tip-off for 300-nautical-mile nominal orbit.	Figures 8 and 9
6. Orbital-altitude error band for a 300-nautical-mile injection altitude and an injection velocity 2 percent greater than circular. ($V_i/V_c = 1.02$)	Figure 10, Table V
7. Effect of injection velocity greater than circular on apogee- and perigee-altitude errors for an injection altitude of 300 nautical miles.	Figure 11
8. Apogee- and perigee-altitude points for nominal injection altitude of 300 nautical miles.	Figure 12

Discussion of Data

The results obtained with regard to the topics summarized above are discussed in the following paragraphs:

1. The 95-percent probability bands for three nominal circular orbits are presented in figure 7. The 300-nautical-mile nominal orbit is the same as the solid boundaries of figure 4. The width of the error band (fig. 7) is seen to increase as the nominal altitude is increased from 120 to 600 nautical miles. It is significant that the maximum spread of the bands occurs near the range angles of 90° and 270° as this indicates the existence of relatively large errors at injection in the flight-path angle. Errors in injection angle tend to have the largest effect on the bands at angles near 90° and 270° whereas errors in the injection velocity have their largest effect near $\phi = 180^\circ$. It is also important to note that the minimum variation in altitude occurs at the point of

injection ($\phi = 0^{\circ}$). More discussion is included about these several points later in the text.

2. The 2σ variations in the injection altitude, velocity, and flight-path angle for the three nominal orbits are listed in table II. These are the RSS values of the variation of the injection parameters for all the error sources which have been obtained by averaging the plus and minus variations. The $(\Delta h)_{2\sigma}$ and $(\Delta\gamma)_{2\sigma}$ values are seen to increase for the higher nominal orbital altitudes while $(\Delta V)_{2\sigma}$ varies only slightly. The larger variations in altitude and flight path are primarily a result of the increasing third-stage coast time as the orbital altitude is increased.

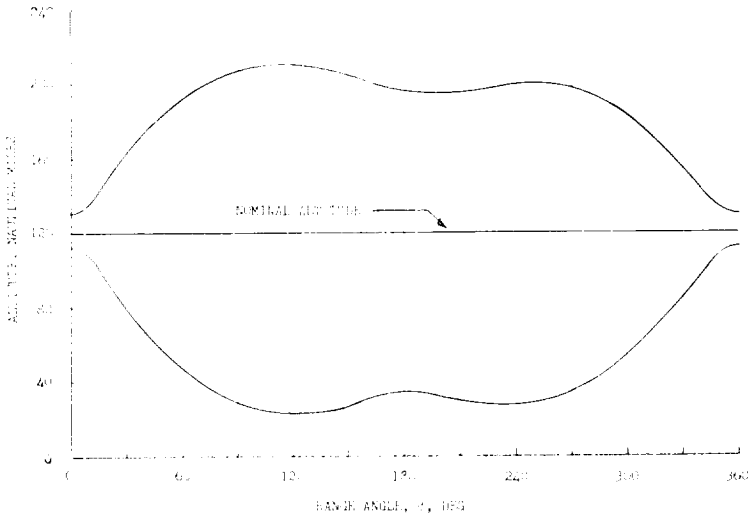

(a) 120 nautical miles.

Figure 7.- The 2σ altitude band for nominal circular orbits.

3. Table III is a tabulation of the separate effects on velocity, altitude, and flight-path angle of each error source at second-, third-, and fourth-stage ignition for the 300-nautical-mile nominal circular mission. As mentioned previously, stage ignition times were held fixed for all the cases, hence this is a listing of the variations at equal times along the trajectory. The case numbers, 1 to 26, refer to the error numbers of table I. The a and b of each case denote the results for the $+2\sigma$ and -2σ value of the errors, respectively.

4. Table IV presents a breakdown of the orbital-altitude variations at the range-angle increments for each error source for the 300-nautical-mile nominal orbit and the RSS values for $(\Delta h)_{+2\sigma}$ and $(\Delta h)_{-2\sigma}$. It also presents a tabulation of the separate effects on velocity, altitude, and flight-path angle of each error source at fourth-stage burnout. There are several points worth noting in this table. First, as mentioned previously, notice that the cases where a relatively large $\Delta\gamma$ exists at injection have the largest Δh at range angles of 90° and 270° (see case 19, for example). On the other hand, for the cases with large ΔV values and relatively small $\Delta\gamma$ values at injection the largest variations in the orbital altitude occur near 180° (see cases 4 and 12, for example). Also from this table the predominant error sources can easily be selected. The largest single variation in orbital altitude is seen to result from the tip-off error (case 19). Also sizable variations occur for most of the rocket parameters particularly for the specific-impulse variations (cases 1 through 4) and propellant-weight errors (cases 9 through 12).

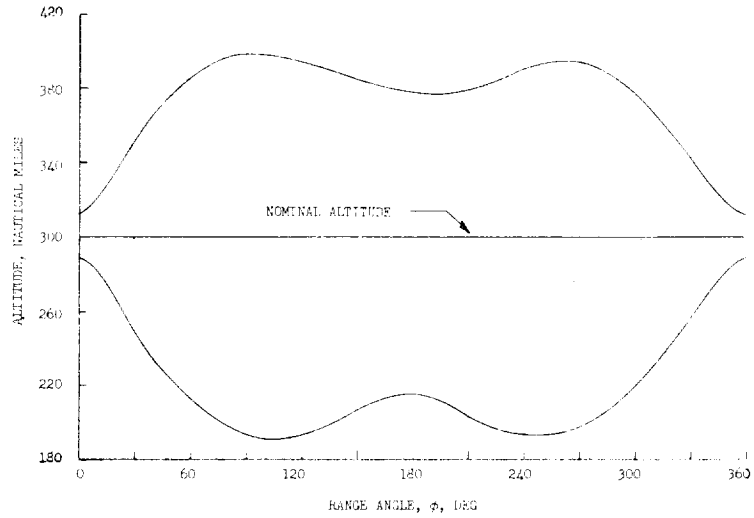

(b) 300 nautical miles.

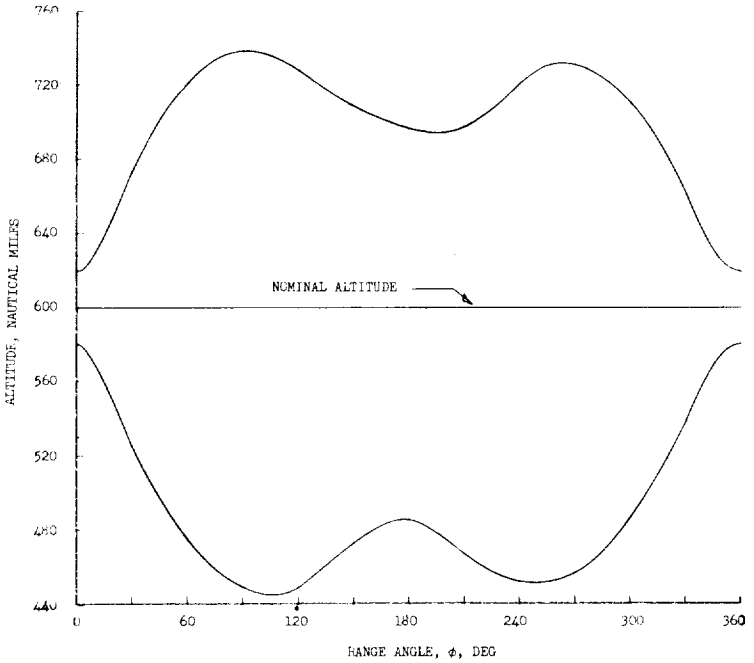

(c) 600 nautical miles.

Figure 7.- Concluded.

5. An indication of how tip-off and certain of the rocket parameters affect the total error band for the 300-nautical-mile nominal circular orbit is shown in figure 8. The basic error band is the same 2σ band shown in figure 7(b) and includes all 26 errors. The dashed boundaries show the resulting band when the tip-off is assumed to be zero. The triangular symbol points form a band which represents the effect of nine motor performance parameters. The nine errors making up the Δ points were specific impulse and propellant weight for all four stages and propellant flow rate for the first stage. The band resulting from these nine errors approximates closely the basic error band without tip-off. Furthermore, it can be seen that only these nine errors plus tip-off (circular symbol points) approximate the basic band, for which all the errors were included, very closely. While an examination of table IV indicates that there are errors equally as important as some of the nine considered, such as drag (case 21) and first-stage thrust misalinement (case 15), the rocket parameters only were chosen to illustrate a significant point. That is, the results presented in figure 8

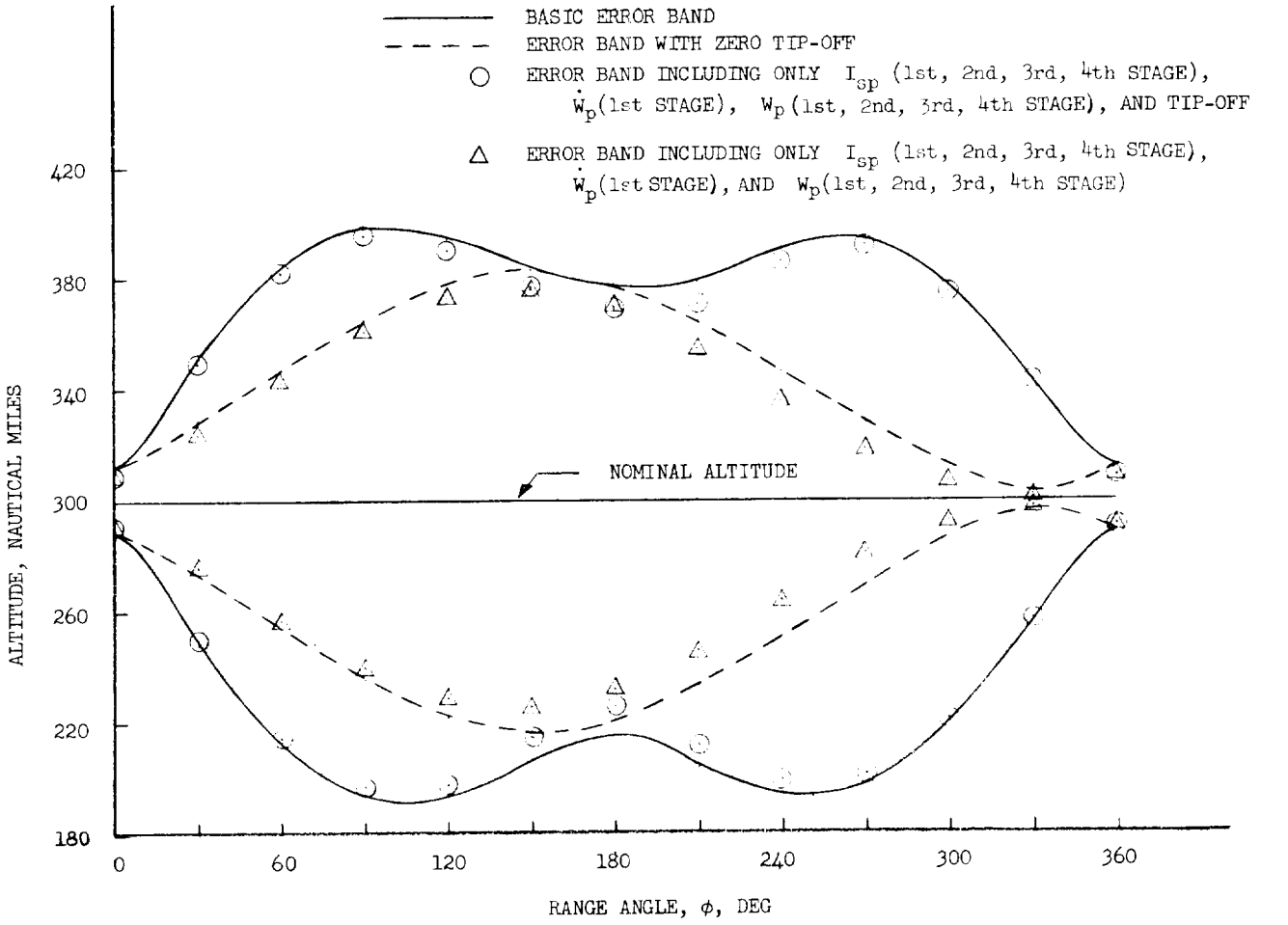

Figure 8.- Effect of rocket parameters and tip-off on basic error band. 300-nautical-mile nominal circular orbit.

indicate that the overall orbital accuracy of the Scout cannot be significantly improved until the rocket parameters can be better defined than those assumed for this analysis. This immediately raises the question as to the validity of the standard deviations assumed for these parameters. Some comparisons of the assumed values for these errors used in the error analysis with ground firings and flight results are presented in appendix C. No conclusions may be drawn, however, due to the questionable accuracy of some of the flight data and the limited number of flight-test data points.

Since a practical estimate of the 2σ value for the tip-off error is unavailable at this time for the present fourth-stage separation system, the effect on the error band of various values of tip-off has been computed and is presented in figure 9. Notice that up to about 2° of tip-off, the maximum uncertainty (maximum spread) of the orbital altitude is little affected by tip-off. For tip-off equal to 4° the maximum altitude variation has been significantly increased, and two

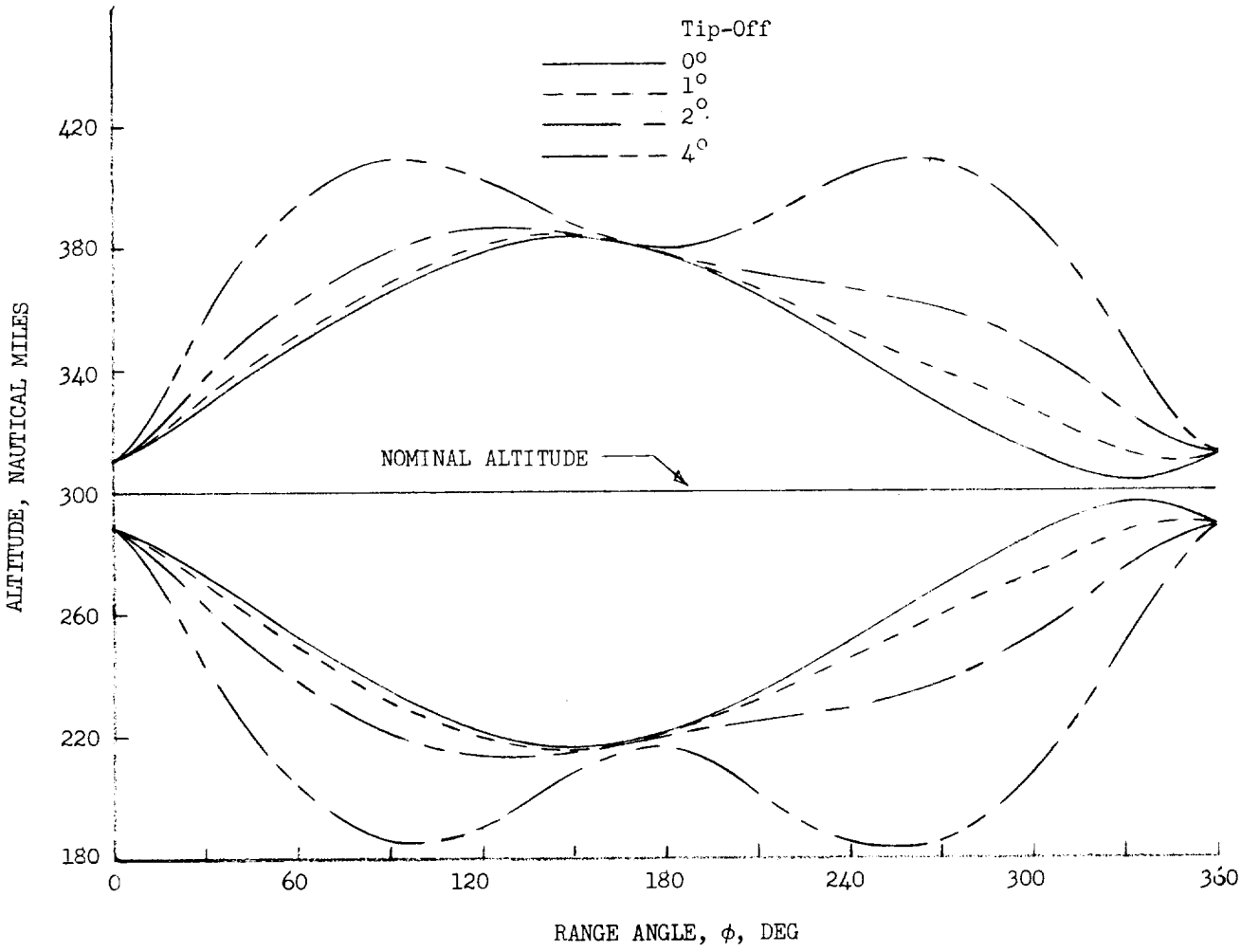

Figure 9.- The 2σ altitude band for various values of tip-off. 300-nautical-mile nominal circular orbit.

maxima occur, as mentioned earlier, as a result of the relatively large error in injection angle produced by the tip-off angle. Thus the maximum uncertainty in orbital altitude on a 95-percent basis, if the nominal mission is a 300-nautical-mile circular orbit, is about ±85 nautical miles for 2σ values of tip-off up to 2°. For a 2σ value of tip-off of 4° the maximum uncertainty for the same mission is about ±110 nautical miles.

6. Up to this point only circular orbits and the expected variations from the circular orbital altitude have been discussed. Attention was called previously in the text to the small variations in orbital altitude occurring at the point of injection (see fig. 7). This fact is significant if, for a given orbital mission, the primary objective is not necessarily an exact circular orbit but the attainment of a minimum altitude within some relatively close tolerance. Figure 10 illustrates how the small variations about the injection point may be used to reduce the perigee altitude uncertainty if slightly elliptical orbits are considered. This figure presents the 2σ altitude band for a nominal injection altitude of 300 nautical miles and a nominal injection velocity V_i equal to 2 percent greater than the circular velocity V_c at 300 nautical miles. The resulting nominal orbit has a 300-nautical-mile perigee altitude and a 615-nautical-mile apogee altitude. The error band then indicates for this nominal that 95 percent

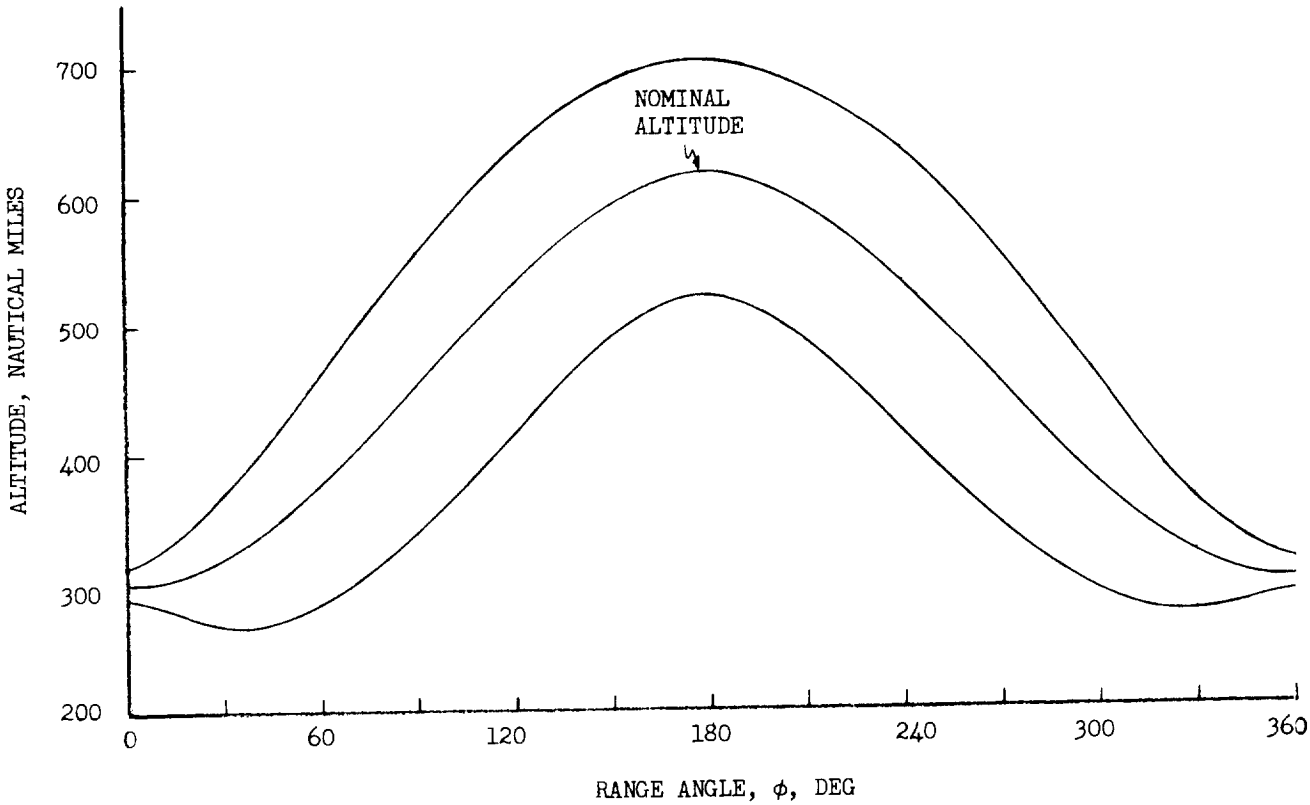

Figure 10.- The 2σ altitude band for 300-nautical-mile nominal injection altitude and $V_i/V_c = 1.02$.

of the time the perigee of the orbit will not be lower than 265 nautical miles. The band also shows that the perigee might be as high as 313 nautical miles. The 2σ uncertainties about the apogee altitude are seen to be about plus 85 nautical miles and minus 95 nautical miles. The 265-nautical-mile perigee altitude should be compared with the results of figure 7(b) where for the circular mission the perigee altitude might occur as low as about 190 nautical miles. The effect of injecting with a velocity greater than the circular velocity is that the injection point tends to be established as the perigee of the orbit and the accuracy as demonstrated in figure 7(b) at the point of injection tends to become the variation about the perigee. The actual uncertainty about the perigee is dependent on the value of the ratio of the injection velocity to the circular value. That is, notice in figure 10, that the perigee of the orbit might occur at a range angle some 40° from the injection point and vary from the nominal perigee by as much as 35 nautical miles. Higher values of V_i/V_c will move the perigee point closer to the injection point and therefore further reduce the perigee-altitude variations.

Table V presents a breakdown of the orbital-altitude variation Δh at the range-angle increments for each separate error source for a nominal 300-nautical-mile injection altitude with $V_i/V_c = 1.02$. The predominant error sources may again be selected as in table IV.

7. The 2σ perigee- and apogee-altitude variations as a function of V_i/V_c for a nominal injection altitude of 300 nautical miles are presented in figure 11. Two sets of curves are presented; the h_a and h_p curves and scale on the right show the apogee and perigee altitudes resulting for the values of V_i/V_c from 1.00 to 1.05 and the $(\Delta h_a)_{2\sigma}$ and $(\Delta h_p)_{2\sigma}$ curves and scale on the left present the apogee-altitude and perigee-altitude variations for the same values of V_i/V_c.

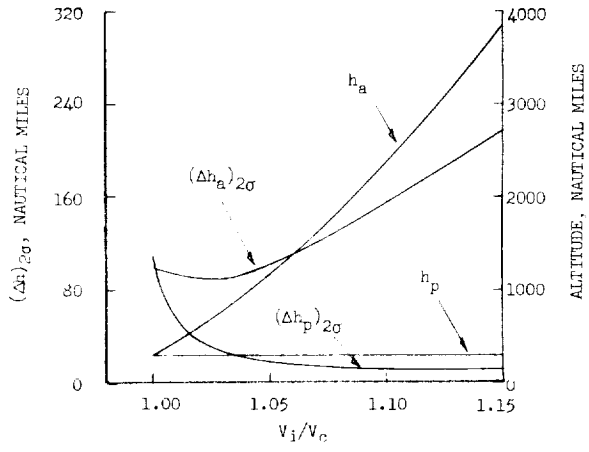

Figure 11.- Effect of injection velocity greater than circular on 2σ apogee- and perigee-altitude variation for an injection altitude of 300 nautical miles.

The V_i/V_c value of 1.00 is the circular case and the 2σ altitude uncertainties with respect to the apogee and perigee altitude possible are those from figure 2(b). The $V_i/V_c = 1.02$ points are those from figure 10. The main point to be noted here is the large decrease in the probable variation about the perigee altitude as the injection velocity is increased. For example, the 2σ altitude variation about the perigee altitude for $V_i/V_c = 1.05$ is seen to be about 20 nautical miles as compared with 110 nautical miles for the circular case ($V_i/V_c = 1.00$). The probable variation of apogee altitude is seen to increase with increasing values of V_i/V_c, but is probably not too critical since the apogee altitudes are also relatively large.

8. The Monte Carlo process provided information on the pairing of apogee and perigee altitudes for each of 200 orbits. These apogee-perigee plots are of more importance to the payload designer, who is more concerned with orbital lifetime and therefore the combination of apogee and perigee altitudes likely to occur, than the altitude band curves (such as fig. 7) which only provide information on the altitude limits likely to occur. Therefore a brief investigation was conducted to provide the payload designer with some boundaries in the apogee-perigee plane that could be used as an aid in determining orbital lifetime. The apogee and perigee altitudes of each of the 200 orbits and the nominal apogee-perigee altitudes are plotted in figure 12(a) for the circular case and in figure 12(b) for a 2-percent over-velocity case of the same injection altitude where the same injection errors were assumed. For purposes of determining maximum and minimum probable orbital lifetimes it would be desirable to enclose an area on these plots

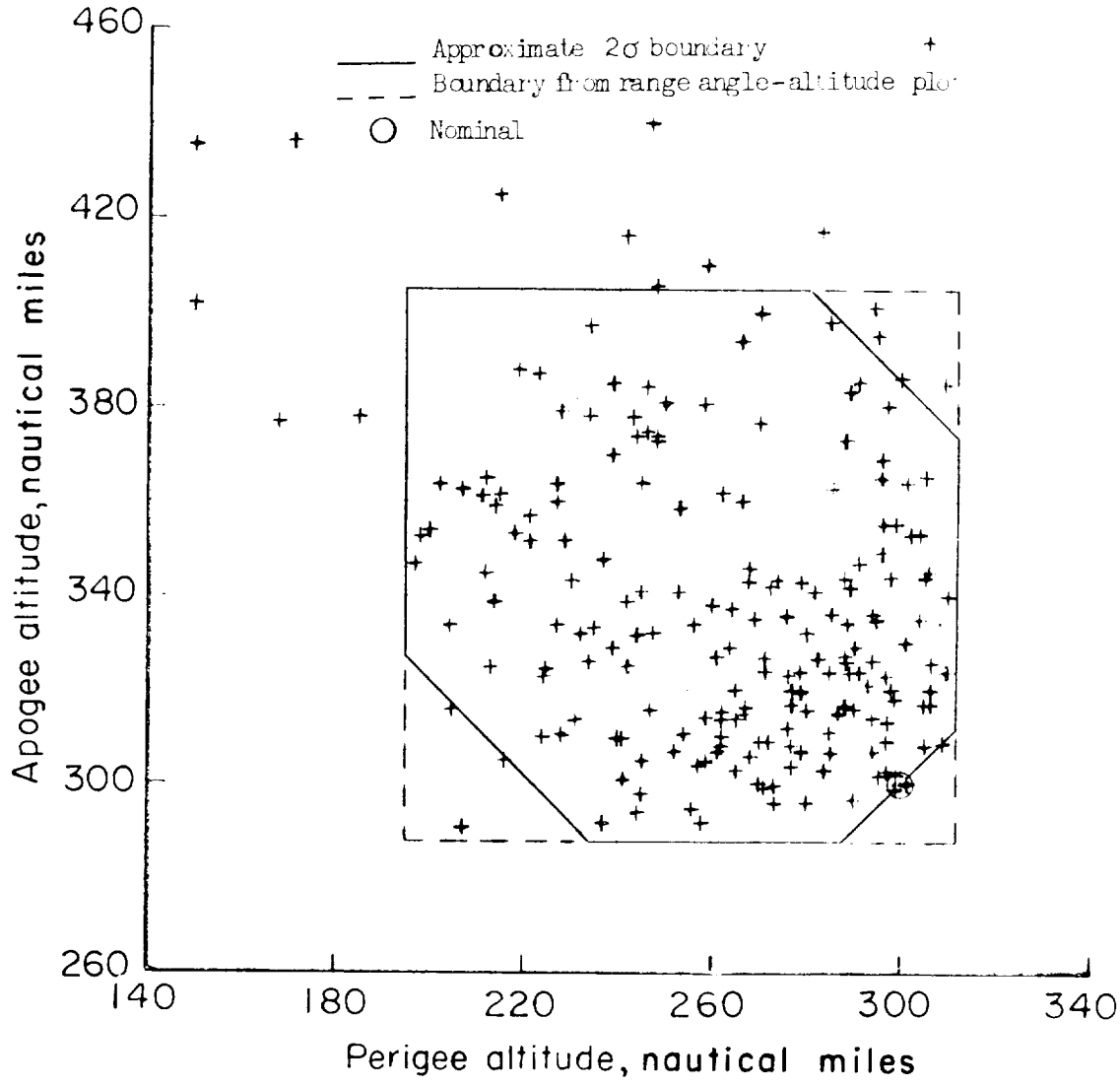

(a) $V_i/V_c = 1.00$.

Figure 12.- Apogee- and perigee-altitude points for nominal injection altitude of 300 nautical miles.

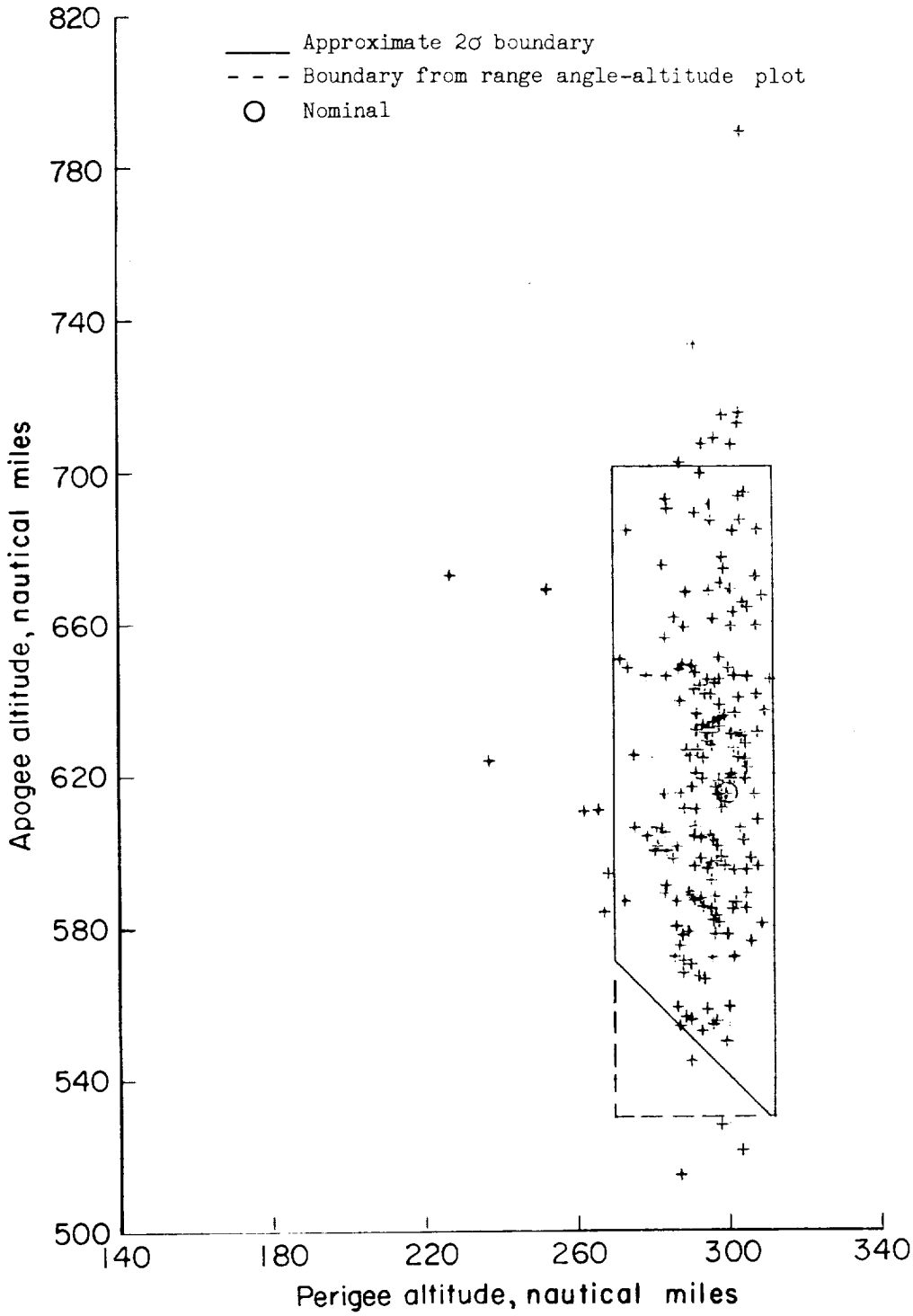

(b) $V_i/V_c = 1.02$.

Figure 12.- Concluded.

within which some percentage, say 95 percent, of all orbits would occur. From the range-angle—altitude plots of figures 7(b) and 10, lines of maximum and minimum perigee and apogee may be determined and plotted on the apogee-perigee plots of figure 12. Maximum-perigee and maximum-apogee altitudes are obtained from the upper altitude band. (These occur at the minimum and maximum altitude, respectively, of the upper altitude band. See sketch.)

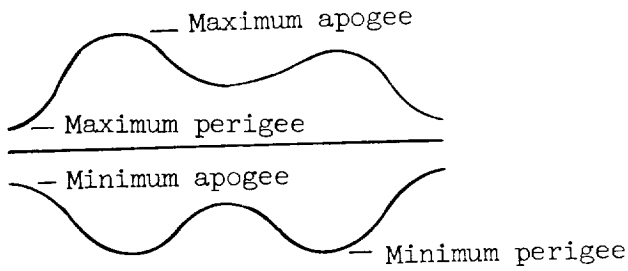

Minimum-perigee and minimum-apogee altitudes are obtained from the lower altitude band (at the minimum and maximum altitude, respectively, of the lower altitude band). Thus, these lines form an enclosed area in the shape of a rectangle. (See the dashed lines in figs. 12(a) and (b).) For the circular case, one corner of this rectangle may be cut off by drawing a 45° line from the origin through the nominal apogee-perigee point. This eliminates the obvious impossibility of having apogee lower than perigee. This area may be further reduced by consideration of the variation in the length of the major axis of the 200 orbits. Since major-axis length is inversely proportional to total energy and total energy would be expected to vary from orbit to orbit, it seems reasonable to expect some variation in major-axis length. Since a 45° line of negative slope through the nominal apogee-perigee point represents the nominal major-axis length, if some statistical variation in major-axis length can be determined, the 2σ value of the variation can then be plotted parallel to the nominal major-axis-length line and hopefully cut off the corners of the remaining shape. The probability distribution function of the major-axis-length variation has been plotted on normal probability paper in figure 13. In addition to the circular case, $V_i/V_c = 1.0$, the probability distribution function has been plotted for $V_i/V_c = 1.01$, 1.02, and 1.05. The $V_i/V_c = 1.05$ points can be closely approximated by a straight line, which shows approximately Gaussian distribution for major-axis-length variation, while a straight line could not be said to approximate any of the other cases shown. However, a smooth curve may be faired through each set of points. Then at least for engineering purposes, these curves may be used to find the 2σ variation in orbital major-axis length. Since the 95-percent probability of being within a given apogee-perigee area has been chosen for the example, the value of the variation in major-axis length at 2.5 percent and 97.5 percent is read off the appropriate faired curve of figure 13. This corresponds to eliminating 5 percent of the variations, and these two values are used as the $+2\sigma$ and -2σ variations in orbital major-axis length. For the circular case, these values were determined to be +86 and -68. Applying these deltas to the nominal major-axis length and plotting the resulting lines of constant major-axis length in figure 12(a) results in cutting off the corners of the area remaining, thus further reducing the area. The preceding analysis was also applied to the $V_i/V_c = 1.02$

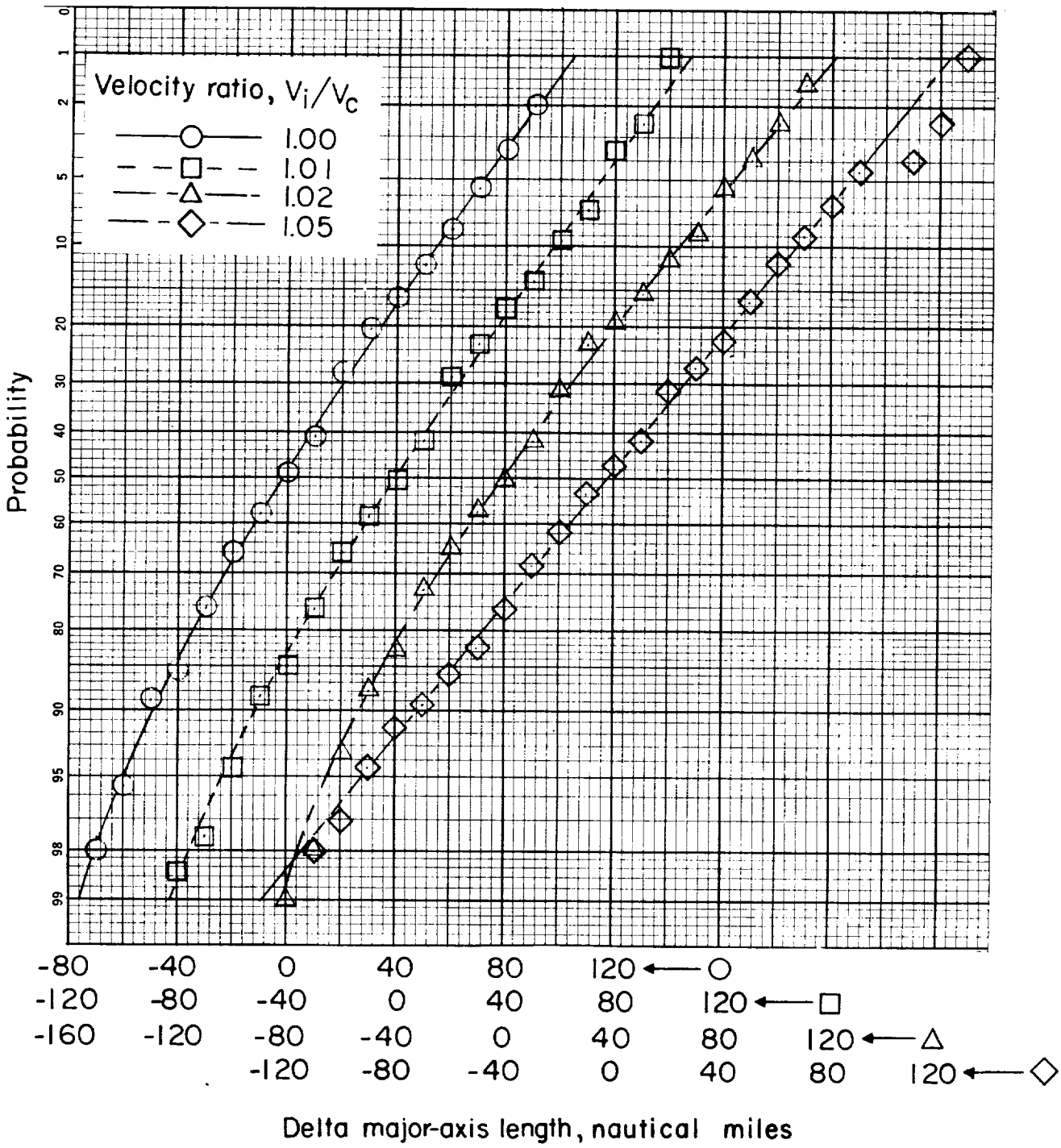

Figure 13.- Probability distribution of the variation of the orbital major-axis length for four ratios of injection velocity to circular velocity.

case resulting in the boundaries shown in figure 12(b). However, it should be recognized that two different methods of analysis have been used in determining this final area. Therefore, depending on the degree of correlation in the two methods, the probability associated with the bounds on the final area might be anywhere from 90.25 percent to 95 percent. For example, in both the circular and the $V_i/V_c = 1.02$ case, more than 10 apogee-perigee points, that is, more than 5 percent are outside the enclosed area, and thus the bounds may not be truly 2σ boundaries. However, the enclosed area does seem reasonable enough to be used in estimating lifetime probabilities.

CONCLUDING REMARKS

A statistical error analysis has been made of the orbital-accuracy capability of the Scout research vehicle. Results are presented in the form of 95-percent probability or $\pm 2\sigma$ orbital-attitude error bands for three nominal circular orbits at altitudes of 120, 300, and 600 nautical miles. In addition, for the 300-nautical-mile mission, a detailed examination was made of the effects of the separate errors, predominant error sources were determined, and an analysis was made of the effect on the orbital accuracy of injecting into the orbit with a velocity greater than that for circular. Also, a method for determining an enclosed area in apogee-perigee space within which approximately 95 percent of all orbits will occur is described and applied to the 300-nautical-mile mission. The enclosed area is considered suitable for use as an aid to determining approximate minimum and maximum orbital lifetime.

The results indicate that the $\pm 2\sigma$ error bands for the 120-, 300-, and 600-nautical-mile nominal circular orbits have maximum variations from the nominal altitudes of approximately ± 100, ± 110, and ± 150 nautical miles, respectively. It was found that these bands are critically dependent upon the fourth-stage tip-off error and will be appreciably less if the present fourth-stage separation system is found to have a 2σ value of tip-off less than the 3.5° assumed in this analysis. For the 300-nautical-mile circular orbit mission, for example, the maximum uncertainty in orbital altitude of a 95-percent basis is reduced to ± 85 nautical miles for a 2σ value of tip-off of about 2°. The results also indicate that the overall accuracy of the Scout vehicle cannot be significantly improved, exclusive of tip-off, until the rocket parameters such as specific impulse, propellant weight, and propellant burning rate, can be defined to within smaller variations than those assumed for this analysis.

Various schemes for improving Scout orbital accuracy have been proposed and investigated by the Scout Project Group at the NASA Langley Research Center. One simple scheme to reduce the uncertainties about the minimum orbital altitude is to inject into orbit with a velocity greater than that for circular. For example, the uncertainty about the minimum altitude in the case of injecting into orbit at an altitude of 300 nautical miles is cut in half by using an over velocity of

1 percent. The attractiveness of this scheme is that in contrast to some others, such as velocity control, modifications to the vehicle are not necessary; however, it is costly in terms of payload.

Langley Research Center,
National Aeronautics and Space Administration,
Langley Station, Hampton, Va., February 5, 1963.

APPENDIX A

EQUATIONS OF MOTION

Differential equations:

$$\dot{V} = \frac{1}{m}\left[F_X \cos \alpha + F_Z \sin \alpha - \left(\frac{R}{r}\right)^2 W \sin \gamma\right]$$

$$\dot{\gamma} = \dot{\phi} + \frac{1}{mV}\left[F_X \sin \alpha - F_Z \cos \alpha - \left(\frac{R}{r}\right)^2 W \cos \gamma\right]$$

$$\ddot{\theta} = \dot{q} = \frac{M_Y}{I_Y}$$

$$\dot{h} = V \sin \gamma$$

$$\dot{\phi} = \frac{V \cos \gamma}{r}$$

$$\dot{L} = \frac{V \cos \gamma \cos \psi}{r}$$

$$\dot{\lambda} = \frac{V \cos \gamma \sin \psi - \omega \cos L}{r \cos L}$$

$$\dot{W} = -\frac{T}{I_{sp}}$$

(See fig. A1.)

Auxiliary equations:

$$F_X = F_{a_X} + F_{T_X}$$

$$F_Z = F_{a_Z} + F_{T_Z} + F_{c_Z}$$

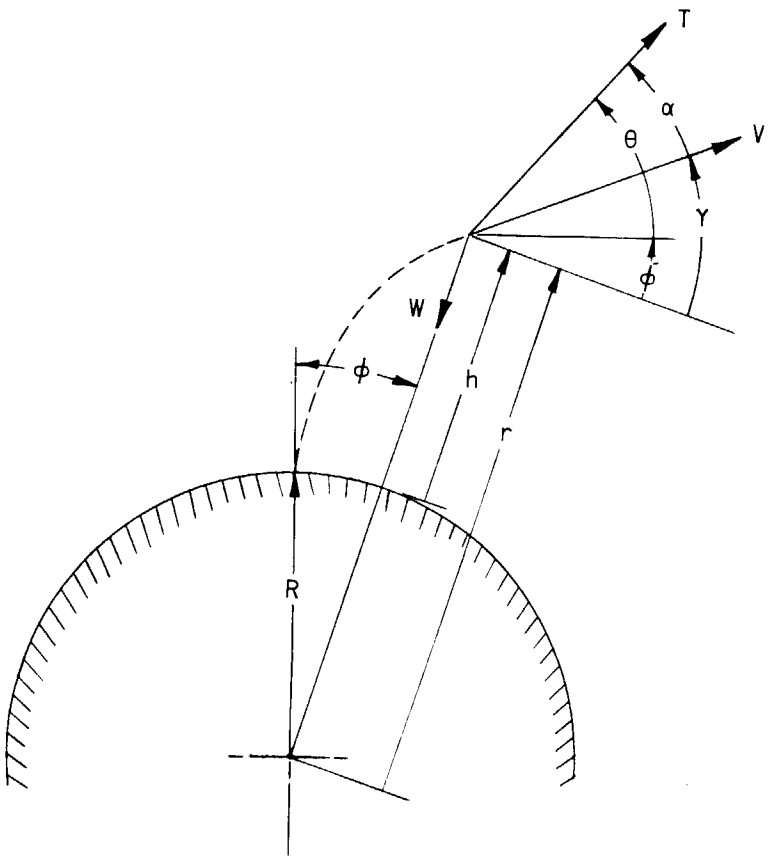

Figure A1.- Basic coordinate system.

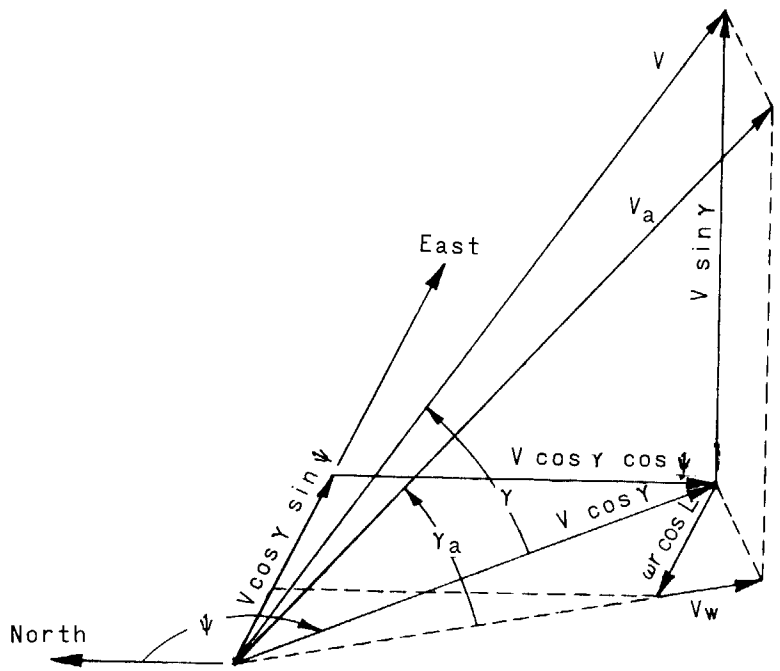

Figure A2.- Aerodynamic flight-path angle and velocity geometry.

$$M_Y = M_{a_Y} + M_{T_Y} + F_{c_Z}\left(x_j - x_{cg_o}\right) + F_Z\left(x_{cg_o} - x_{cg}\right)$$

$$F_{a_X} = -\bar{q}C_A S$$

$$F_{a_Z} = -\left[\bar{q}C_N S + \left(\bar{q}C_{N_\delta} S + F_{\delta_v}\right)\delta\right]$$

$$M_{a_Y} = \bar{q}C_m dS + \frac{C_{m_q} S\rho V_a d^2\dot{\theta}}{4} + \left(\bar{q}C_{m_\delta} dS - F_{\delta_v} x_v\right)\delta$$

$$F_{T_X} = T' \cos \tau$$

$$F_{T_Z} = T' \sin \tau$$

$$M_{T_Y} = T'b$$

$$r = R + h$$

$$V_a = \left[(V \sin \gamma)^2 + \left\{\left[(V \cos \gamma \sin \psi - \omega r \cos L)^2 + (V \cos \gamma \cos \psi)^2\right]^{1/2} + V_w\right\}^2\right]^{1/2}$$

$$\gamma_a = \tan^{-1}\left\{\frac{V \sin \gamma}{\left[(V \cos \gamma \sin \psi - \omega r \cos L)^2 + (V \cos \gamma \cos \psi)^2\right]^{1/2} + V_w}\right\}$$

(See fig. A2.)

$$M = \frac{V_a}{a}$$

$$\alpha = \phi + \theta - \gamma$$

$$\alpha_a = \phi + \theta - \gamma_a$$

$$T' = T + (2116 - P)A_e$$

$$\left.\begin{aligned} \sin \psi &= \frac{\cos i}{\cos L} \\ \cos \psi &= -\sqrt{1 - \sin^2 \psi} \end{aligned}\right\}$$ NOTE: Implicit in these equations is a due east launch requirement in the northern hemisphere.

Control equations:

First stage -

$$\delta = K_\theta(\theta - \theta_c) + K_{\dot\theta}\dot\theta$$

Second stage -

$$\epsilon = K_\theta(\theta - \theta_c) + K_{\dot\theta}\dot\theta$$

$$F_{c_Z} = 0, \quad |\epsilon| \leqq \Delta_c$$

$$F_{c_Z} = -T_j, \quad \epsilon > \Delta_c$$

$$F_{c_Z} = T_j, \quad \epsilon < -\Delta_c$$

Tabular inputs:

Function of time - T, F_{δ_V}, θ_c

Function of weight - x_{cg}, I_Y

Function of altitude - V_w, ρ, P, a

Function of Mach number and α_a. C_A, C_N, C_m, C_{m_q}, C_{N_δ}, C_{m_δ}

APPENDIX B

MONTE CARLO ANALYSIS

The Monte Carlo results are based on the same set of velocity, altitude, and flight-path-angle injection errors (the 300-nautical-mile injection errors listed in table IV) as the root sum square (RSS) results. The difference thereafter is in the different method of treating the injection errors to obtain the altitude variation about the nominal at the various range angles. The method of obtaining the RSS results has previously been described. The Monte Carlo analysis was conducted as follows:

1. The plus and minus 3σ injection errors were plotted for each of the 26 error sources and a quadratic fitted through these points and the zero points (see sketch).

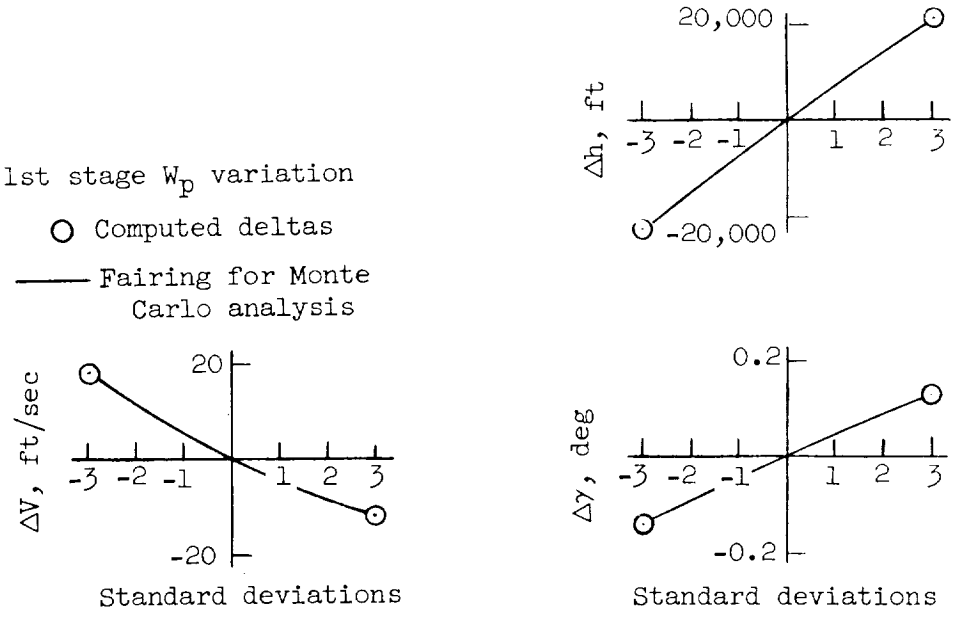

The resulting quadratic coefficients for Δh, ΔV, and $\Delta\gamma$ are shown in the following table where

$$\left.\begin{aligned} \Delta h_j &= b_j\lambda + a_j\lambda^2 \\ \Delta V_j &= b'_j\lambda + a'_j\lambda^2 \qquad j = 1, \ldots, 26 \\ \Delta\gamma_j &= b''_j\lambda + a''_j\lambda^2 \end{aligned}\right\} \tag{B1}$$

and λ is the number of standard deviations. The j subscript is used to

identify the error source. It should be noted in the following table that many of the a coefficients are zero, thus indicating that normal distribution of the error was assumed.

Error	Δh		ΔV		$\Delta \gamma$	
	a_j	b_j	a'_j	b'_j	a''_j	b''_j
1	0	0.167×10^5	0	0.333×10	0	0.910×10^{-1}
2	0	$.150 \times 10^5$	0	$.176 \times 10^2$	0	.106
3	0	$.125 \times 10^5$	0	$.239 \times 10^2$	0	.102
4	$.410 \times 10^2$	$.147 \times 10^2$	0	$.164 \times 10^2$	0	$.280 \times 10^{-2}$
5	$-.243 \times 10^3$	$.295 \times 10^4$	0	$.140 \times 10^2$	0	$-.112 \times 10^{-1}$
6	0	$.455 \times 10^4$	0	$-.685 \times 10$	0	$.135 \times 10^{-1}$
7	0	$.464 \times 10^4$	0	$-.567 \times 10$	0	$.180 \times 10^{-1}$
8	0	$.200 \times 10^3$	0	.670	0	$.870 \times 10^{-2}$
9	$-.106 \times 10^3$	$.728 \times 10^4$	.306	$-.488 \times 10$	0	$.457 \times 10^{-1}$
10	0	$.286 \times 10^4$	0	$.866 \times 10$	0	$.292 \times 10^{-1}$
11	$.282 \times 10^3$	$.963 \times 10^3$	.492	$.787 \times 10$	0	$.170 \times 10^{-1}$
12	0	$-.262 \times 10^4$	0	$.150 \times 10^2$	0	$-.190 \times 10^{-1}$
13	$.119 \times 10^3$	$-.251 \times 10^3$	0	-.313	$.720 \times 10^{-3}$	$.150 \times 10^{-2}$
14	0	$.750 \times 10^4$	-.246	$-.164 \times 10^2$	0	$.460 \times 10^{-1}$
15	$-.989 \times 10^2$	$.532 \times 10^4$	0	$-.191 \times 10^2$	$.700 \times 10^{-3}$	$-.180 \times 10^{-2}$
16	$.569 \times 10^3$	$.116 \times 10^5$	-.842	$-.238 \times 10^2$	0	$.330 \times 10^{-1}$
17	$.105 \times 10^4$	$.118 \times 10^5$	-.547	$-.202 \times 10^2$	0	$.462 \times 10^{-1}$
18	$.107 \times 10^4$	$-.548 \times 10^4$	$-.228 \times 10$	.690	0	$-.232 \times 10^{-1}$
19	$-.164 \times 10^3$	$.444 \times 10^4$	$-.231 \times 10$	$-.170 \times 10^2$	0	.665
20	0	$.195 \times 10^3$	0	-.540	0	$.292 \times 10^{-1}$
21	0	$-.110 \times 10^5$	-.428	$-.346 \times 10$	0	$-.628 \times 10^{-1}$
22	$.412 \times 10^2$	$.415 \times 10^2$	$.890 \times 10^{-2}$	$.267 \times 10^{-1}$	$-.278 \times 10^{-3}$	$-.167 \times 10^{-3}$
23	0	$-.977 \times 10^3$	0	-.190	0	$-.530 \times 10^{-2}$
24	0	$-.193 \times 10^4$	0	$-.171 \times 10$	0	$-.128 \times 10^{-1}$
25	0	$-.177 \times 10^4$	0	$-.284 \times 10$	0	$-.138 \times 10^{-1}$
26	0	$-.595 \times 10^3$	0	$-.108 \times 10^2$	0	$-.620 \times 10^{-2}$

Example: $\Delta h = a_j\lambda^2 + b_j\lambda$ where λ is a normally distributed random number.

2. Total injection errors in h, V, and γ were determined by generating 26 random values of λ, representing each of the 26 error sources, where λ was assumed to be normally distributed, and inserting these random values of λ into equations (B1). This resulted in 26 sets of Δh_j, ΔV_j, and $\Delta\gamma_j$ which when summed algebraically represented the total injection errors for one orbit, that is,

$$\left.\begin{aligned} \Delta h_t &= \sum_{j=1}^{26} \Delta h_j \\ \Delta V_t &= \sum_{j=1}^{26} \Delta V_j \\ \Delta\gamma_t &= \sum_{j=1}^{26} \Delta\gamma_j \end{aligned}\right\} \tag{B2}$$

The off-nominal injection conditions then are

$$\left.\begin{aligned} h_i &= h_{nom} + \Delta h_t \\ V_i &= V_{nom} + \Delta V_t \\ \gamma_i &= \gamma_{nom} + \Delta\gamma_t \end{aligned}\right\} \tag{B3}$$

where injection is denoted by the subscript i. This procedure was repeated 200 times to obtain 200 orbits for statistical analysis.

3. At given range angles from injection, the altitude difference Δh between the off-nominal orbit and the nominal orbit was determined for each of the 200 orbits. To determine the statistical nature of the altitude variation, the observed range of Δh at a particular range angle was divided into 20 equal increments and a histogram of the number of occurrences of Δh within each increment was constructed. Appropriate integration of the histograms and normalization by the total number of Δh's involved (200) provided the probability distribution function. These distributions were then plotted on probability paper as shown in figure B1. This paper is scaled such that a Gaussian probability distribution will plot as a straight line. As can be seen in figure B1, a straight line is a good fairing of the plotted points thus indicating normal or Gaussian distribution of Δh at each of the range angles. The comparison between

these results and the RSS results has been made on figure 4 and noted to be very good. It should be mentioned that the Monte Carlo analysis was also performed with 100 orbits rather than 200 and much the same results were obtained. Thus 200 orbits would appear to be enough to adequately determine the variation in orbital altitude due to the 26 error sources of table I.

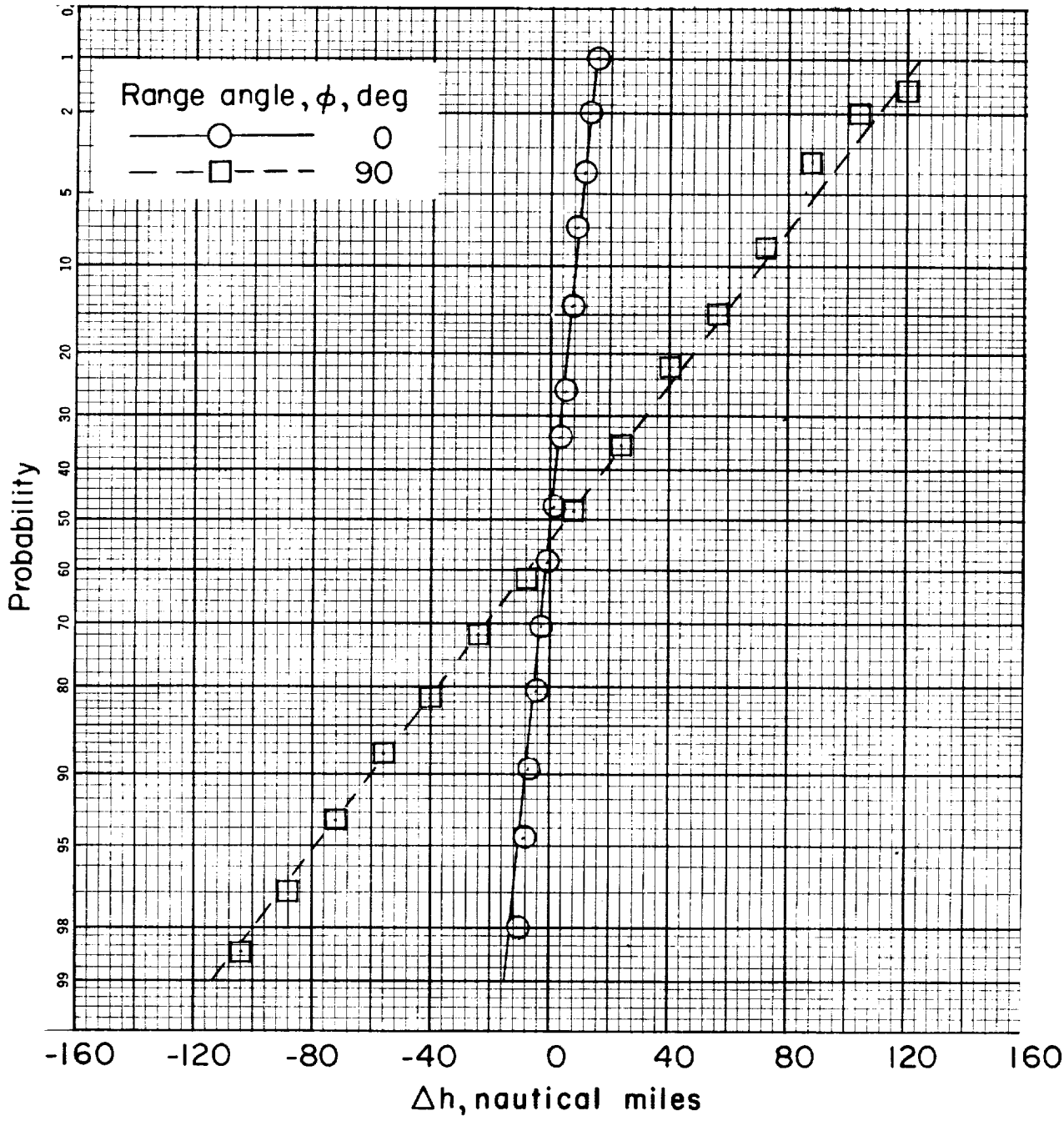

(a) $V_i/V_c = 1.00$; $\phi = 0^\circ$ and 90°.

Figure B1.- Probability distribution of altitude variations at various values of range angle and for two ratios of injection velocity to circular velocity.

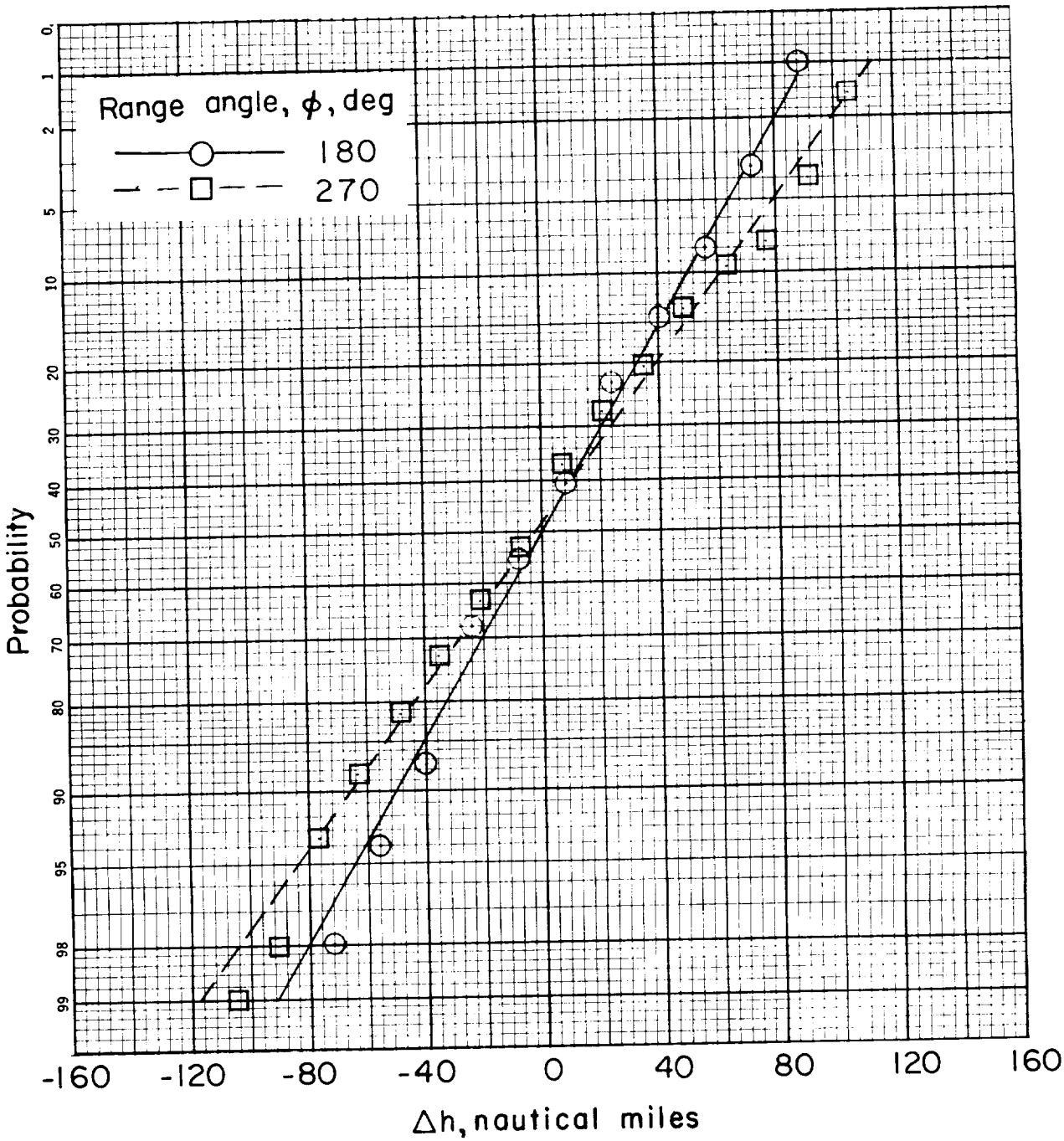

(b) $V_i/V_c = 1.00$; $\phi = 180^\circ$ and 270°.

Figure B1.- Continued.

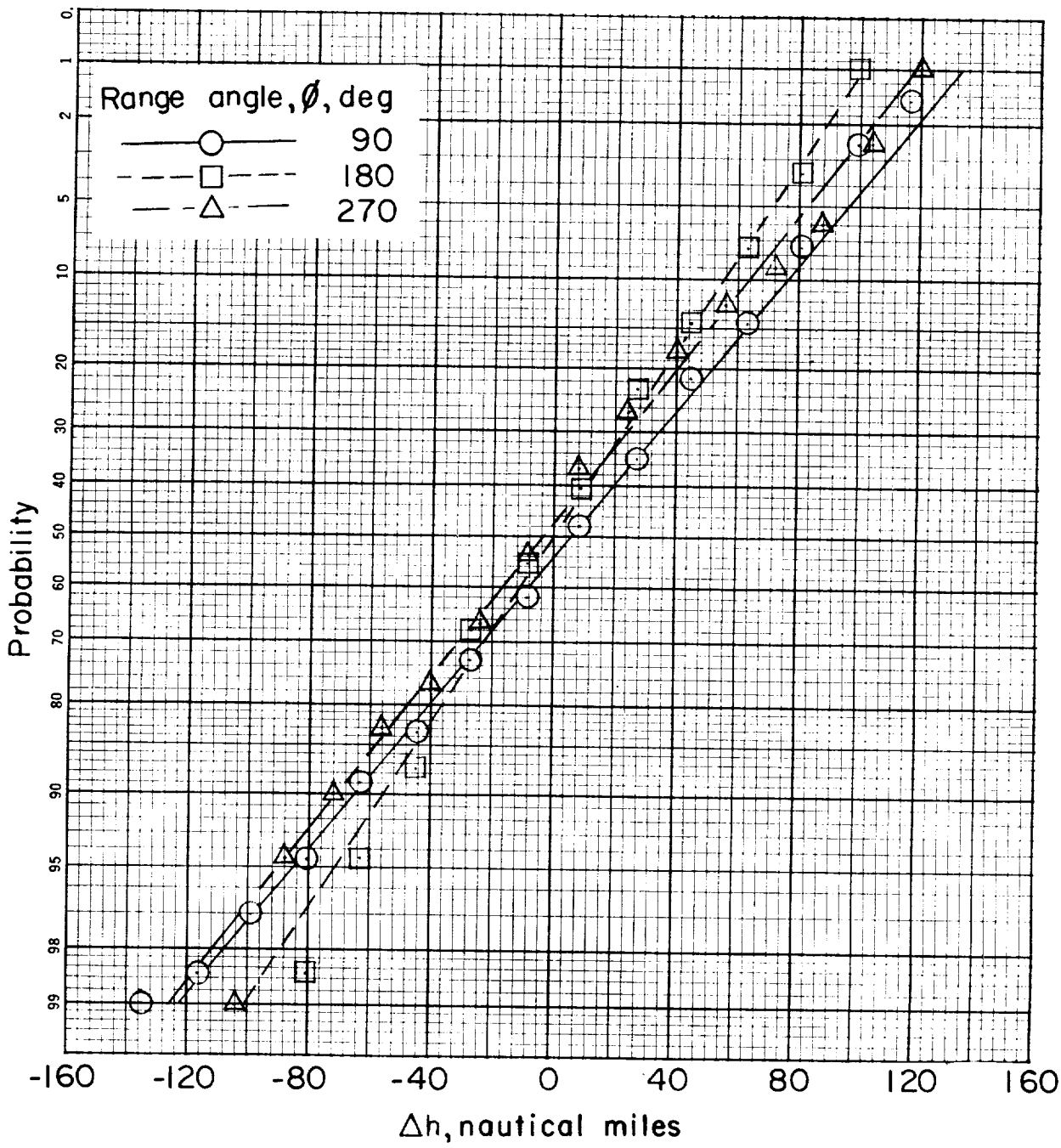

(c) V_i/V_c = 1.02; ϕ = 90°, 180°, and 270°.

Figure B1.- Concluded.

APPENDIX C

COMPARISON OF SOME ERROR-ANALYSIS DATA AND RESULTS WITH FLIGHT RESULTS AND ROCKET-MOTOR GROUND TESTS

Sometime after the standard-deviation values for the rocket-motor parameters were established (assumed) for use in the error analysis, available data of all the ground tests of the Scout motors were collected and analyzed. From these test data, standard-deviation values were determined. It is of interest to compare the 2σ values assumed for the error analysis with the data measured from these ground firings. The following table presents these data. The data are compared

TABLE CI.- COMPARISON OF THE 2σ VALUES OF THE ROCKET-MOTOR PARAMETERS DERIVED FROM GROUND FIRINGS* AND THOSE USED IN THE ERROR ANALYSIS

	Total impulse variation $(\Delta I_t)_{2\sigma}$, percent, for -			
	1st stage motor	2nd stage motor	3rd stage motor	4th stage motor
Error analysis	1.20	1.20	1.20	0.75
Ground tests	.86	1.32	.18	1.08
	Web burnout-time variation $(\Delta t_b)_{2\sigma}$, sec, for -			
	1st stage motor	2nd stage motor	3rd stage motor	4th stage motor
Error analysis	1.07	1.13	1.43	1.17
Ground tests	1.30	1.02	1.92	3.64

*The 2σ values listed as those derived from the ground firings were determined from the following number of runs -

Motor	1st	2nd	3rd	4th
Number of tests	4	10	4	7

for two of the rocket parameters - total impulse and web burnout time. The web burnout time is the time at which the rocket chamber pressure starts trailing off to zero. (See fig. 5(b) at $t = 37$ seconds.) Although the error analysis did not consider these same parameters but rather specific impulse, total propellant weight, and propellant burning rate, still a reasonable comparison is possible.

As explained in the main part of the text, in the analysis the total impulse was affected only by the specific impulse and total propellant-weight errors. The burning time and likewise web burnout time was primarily changed by the propellant burning-rate error. Hence, the 2σ values for the percentage change in total impulse listed in table CI for the error analysis are the statistical sum (RSS) of the variations of total impulse associated with I_{sp} and W_p. The 2σ web burnout-time values listed for the error analysis are the values associated with the 2σ values of $\dot{W}_p$ errors for each stage. In general, the agreement is fair with the exception of $(\Delta I_t)_{2\sigma}$ for the third-stage motor and $(\Delta t_b)_{2\sigma}$ for the fourth-stage motor. Notice the limited number of firings from which the ground tests data were obtained.

A summary has also been made of the differences in total impulse and web burnout time between the values for those measured during the first seven Scout flights and the values predicted for each specific motor for the same flights. These data are presented in figure C1. Figure C1(a) presents the percent difference between the flight measured and preflight predicted total impulse. Figure C1(b) summarizes the differences for the web burnout time. It must be pointed out that the total impulse data measured in flight were obtained by integration of the vehicle longitudinal acceleration and hence the accuracy of the data is affected by a number of factors. First-stage thrust impulse for example was determined by assuming that the vehicle aerodynamic drag is known. For all stages the accuracy of the impulse data is affected by the telemetry, sensor, and read-out accuracy. The web burnout time was obtained in flight from the chamber-pressure time history of the rocket motors and is probably fairly accurate. It is worth noting on figure C1(b) that the first-stage rocket has been consistently burning faster than predicted. That is, the flight web burnout time on all the shots but ST-5 has been less than the predicted value. It is pointed out in the main text that the first-stage burning rate ($\dot{W}_p$) was found to be important. Also an examination of the effect of this error has shown that for an increased burning rate the resulting altitude and flight-path angle will be above the nominal. This has actually been the case for the altitude and path angle measured in flight. The 2σ values of the error analysis (from table C1) are noted on the figures as dashed lines. The discrepancies noted can be attributed at least in part to the lack of motor grain temperature control on the launching pad in the early Scout firings. The launch tower at Wallops Island has since been furnished with equipment capable of motor grain temperature control.

The differences noted between the predicted and flight measured values of velocity, altitude, and flight-path angle at various points along the trajectory for the first seven flights have been tabulated in figure C2. The 2σ variations as predicted by the error analysis are also noted here for comparison. Attempts to correlate the data on figure C2 and the rocket data of figure C1 have exposed many inconsistencies. For example, from figures C1(a) and C1(b) on ST-1 the first-stage flight impulse was less than predicted and the motor burned faster than predicted. Based on the error study, the effect of both of these conditions is to cause a reduction in the velocity of second-stage ignition, yet on figure C2(a) the ΔV is noted to be a small positive value. Due to these inconsistencies, some of which are no doubt due to inaccurate flight data, data-reduction

methods, and the limited number of flights to date, it is felt that insufficient evidence exists to justify changing the value of the 2σ variation assumed for any of the error sources included in the error analysis.

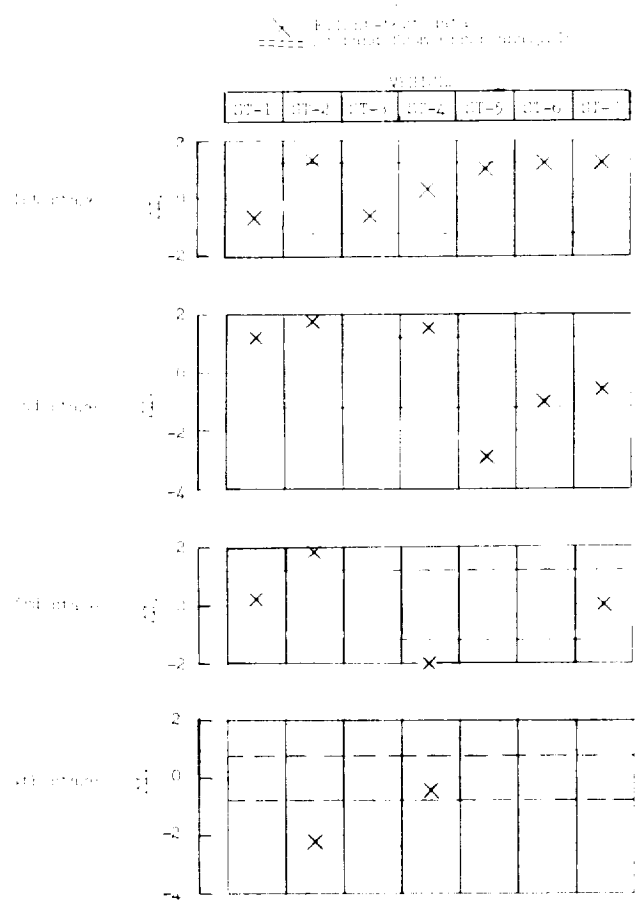

(a) $\Delta I_t = 100 \left(\frac{\text{Flight impulse - Predicted impulse}}{\text{Predicted impulse}} \right)$, percent.

Figure C1.- Differences between flight measured and predicted total impulse and web burnout time.

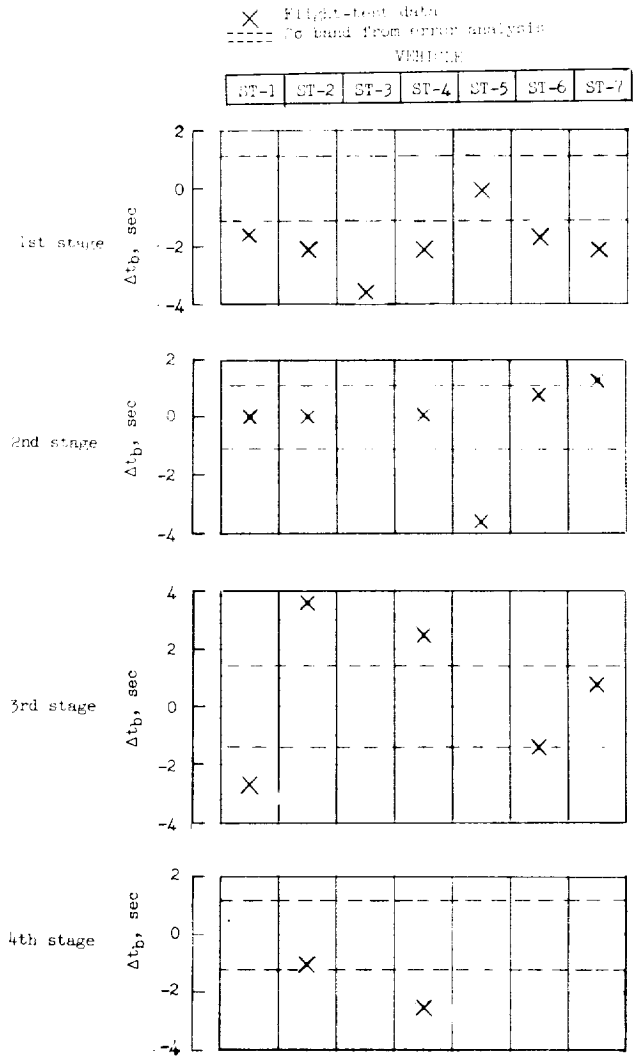

(b) Δt_b = (Flight web burnout time - Predicted web burnout time), seconds.

Figure C1.- Concluded.

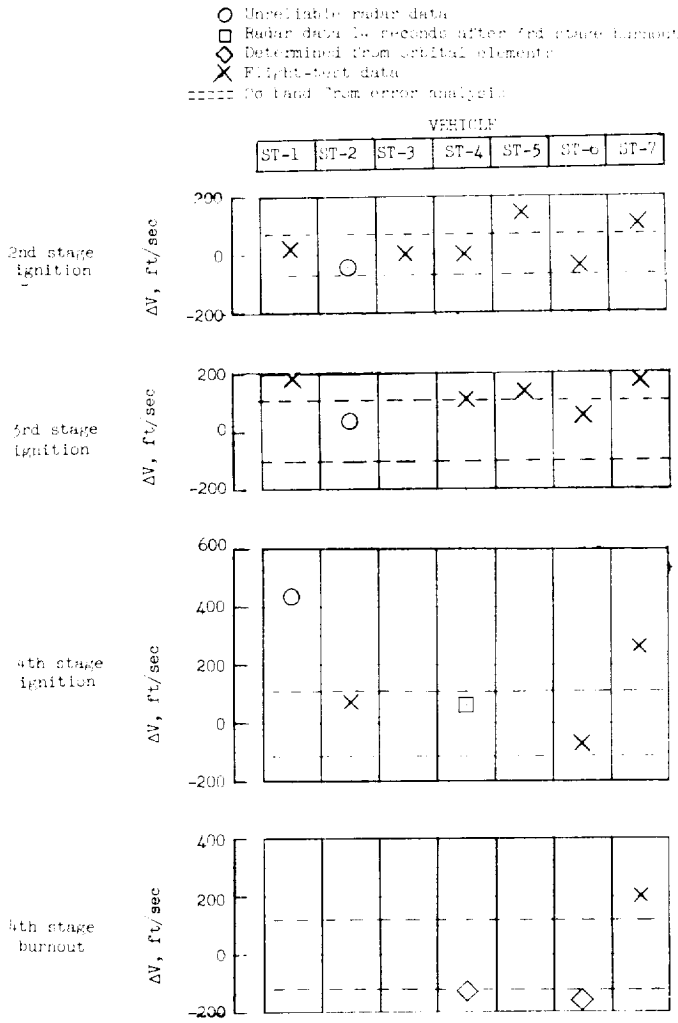

(a) ΔV = (Flight V - Predicted V), ft/sec.

Figure C2.- Differences between flight measured and predicted velocity, altitude, and flight-path angle at various points along the ascent trajectory.

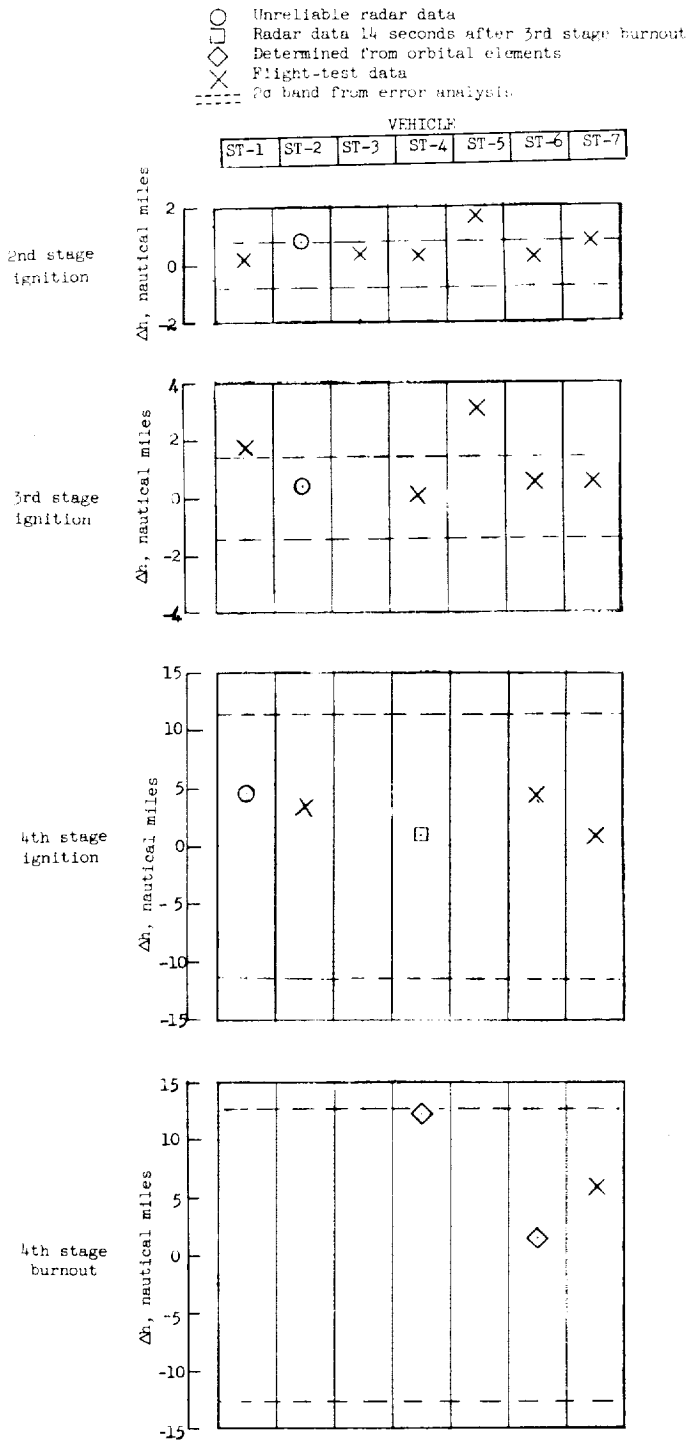

(b) Δh = (Flight h - Predicted h), nautical miles.

Figure C2.- Continued.

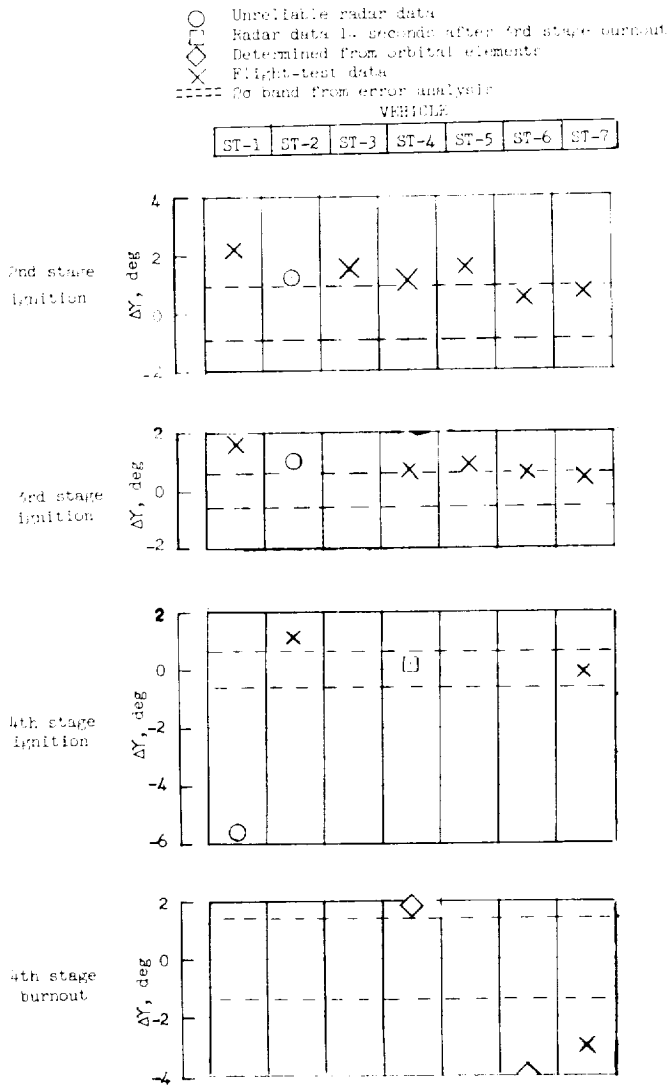

(c) $\Delta\gamma$ = (Flight γ - Predicted γ), deg.

Figure C2.- Concluded.

REFERENCE

1. Young, George R., and Buglia, James J.: An Analysis of the Coning Motions of the Final Stages of Three NASA Scout Development Vehicles. NASA TN D-1396, 1962.

TABLE I.- ERROR SOURCES AND MAGNITUDES USED IN THE ANALYSIS

Case	Error	2σ value
1	1st stage specific impulse	1.0 percent
2	2nd stage specific impulse	1.0 percent
3	3rd stage specific impulse	1.0 percent
4	4th stage specific impulse	0.35 percent
5	1st stage propellant flow rate	3.3 percent
6	2nd stage propellant flow rate	3.3 percent
7	3rd stage propellant flow rate	3.3 percent
8	4th stage propellant flow rate	3.3 percent
9	1st stage propellant weight	0.67 percent
10	2nd stage propellant weight	0.67 percent
11	3rd stage propellant weight	0.67 percent
12	4th stage propellant weight	0.67 percent
13	Launch attitude	0.33°
14	Attitude program	0.13°
15	1st stage thrust misalinement	0.17°
16	2nd stage thrust misalinement	0.13°
17	3rd stage thrust misalinement	0.067°
18	Winds (fig. 6)	200 fps maximum
19	4th stage tip-off	3.5°
20	Dead band	0.15°
21	Drag coefficient	6.7 percent
22	Static margin	Static margin varied one body diameter (40 in.)
23	1st stage dry weight	0.33 percent
24	2nd stage dry weight	0.33 percent
25	3rd stage dry weight	0.33 percent
26	4th stage dry weight	0.33 percent

TABLE II.- 2σ VARIATIONS IN INJECTION PARAMETERS

Nominal circular orbital altitude, nautical miles	$(\Delta h)_{2\sigma}$, nautical miles	$(\Delta V)_{2\sigma}$, ft/sec	$(\Delta \gamma)_{2\sigma}$, deg
120	8.7	135	1.19
300	12.0	125	1.40
600	19.6	140	1.84

TABLE III.- VARIATIONS OF ΔV, Δh, AND $\Delta\gamma$ DUE TO EACH ERROR SOURCE AT SECOND-, THIRD-, AND FOURTH-STAGE IGNITION FOR 300-NAUTICAL-MILE NOMINAL CIRCULAR ORBIT

[The case numbers refer to the error sources of table I; a and b are the $+2\sigma$ and -2σ error values, respectively]

Case	2nd ignition			3rd ignition			4th ignition		
	Δh, ft	ΔV, ft/sec	$\Delta\gamma$, deg	Δh, ft	ΔV, ft/sec	$\Delta\gamma$, deg	Δh, ft	ΔV, ft/sec	$\Delta\gamma$, deg
	h_{nom} = 129,987	V_{nom} = 4,211.5	γ_{nom} = 27.588	h_{nom} = 294,467	V_{nom} = 10,589.6	γ_{nom} = 24.864	h_{nom} = 1,827,697	V_{nom} = 15,409.1	γ_{nom} = -0.015
1-a	2,195	45.5	0.361	4,256	44.2	0.167	30,015	8.9	0.271
1-b	-2,234	-47.0	-.381	-4,361	-46.4	-.173	-30,939	-8.6	-.281
2-a	0	0	0	1,085	69.5	.060	26,679	37.3	.295
2-b	0	0	0	-1,090	-69.9	-.061	-26,822	-37.1	-.299
3-a	0	0	0	0	0	0	21,867	50.0	.276
3-b	0	0	0	0	0	0	-21,701	-49.3	-.277
4-a	0	0	0	0	0	0	0	0	0
4-b	0	0	0	0	0	0	0	0	0
5-a	3,243	-22.7	.311	3,666	-23.1	.113	4,507	-27.8	-.017
5-b	-3,665	21.2	-.369	-4,317	21.0	-.138	-7,663	29.5	-.007
6-a	0	0	0	2,359	-3.0	.087	7,906	-12.8	.045
6-b	0	0	0	-2,595	1.5	-.095	-9,304	13.0	.057
7-a	0	0	0	0	0	0	8,248	-9.6	.057
7-b	0	0	0	0	0	0	-9,091	12.2	-.061
8-a	0	0	0	0	0	0	0	0	0
8-b	0	0	0	0	0	0	0	0	0
9-a	255	25.5	.092	1,076	25.1	.049	12,327	10.0	.124
9-b	-325	-28.1	-.109	-1,250	-28.0	-.057	-13,914	-10.9	-.140
10-a	-393	-8.8	-.067	-828	23.6	-.024	4,643	18.0	.073
10-b	391	8.7	.067	806	-24.7	.023	-5,077	-18.5	-.078
11-a	-113	-2.5	-.019	-390	-14.2	-.018	2,694	19.9	.057
11-b	109	2.3	.019	379	14.0	.018	-180	-13.1	-.025
12-a	-27	-.7	-.004	-93	-3.4	-.004	-4,557	-8.9	-.055
12-b	27	.7	.004	93	3.4	.005	4,575	9.0	.055
13-a	4	-.2	.003	5	.3	.001	-29	-.2	.001
13-b	31	1.9	.007	87	1.8	.003	872	.7	.009
14-a	327	-4.6	.143	1,012	-7.4	.141	13,739	-31.7	.095
14-b	-330	4.6	-.143	-1,020	7.4	-.141	-13,825	31.7	-.096
15-a	1,401	-21.5	.599	2,640	-23.6	.219	9,681	-39.4	.030
15-b	-1,469	18.3	-.590	-2,795	19.6	-.219	-11,183	37.4	-.046
16-a	0	0	0	1,793	-9.5	.396	24,759	-51.4	.174
16-b	0	0	0	-1,374	9.5	-.311	-18,852	42.0	-.128
17-a	0	0	0	0	0	0	27,343	-43.3	.235
17-b	0	0	0	0	0	0	-17,000	37.0	-.130
18-a	-1,270	-14.5	-.218	-2,069	-15.5	-.044	-4,302	-16.4	-.041
18-b	1,770	5.0	.475	3,351	2.8	.201	16,041	-17.3	.112
19-a	0	0	0	0	0	0	0	0	0
19-b	0	0	0	0	0	0	0	0	0
20-a	0	0	0	0	0	0	0	0	0
20-b	0	0	0	0	0	0	0	0	0
21-a	-1,142	-33.8	-.211	-2,493	-33.5	-.100	-19,983	-9.2	-.168
21-b	1,151	34.0	.209	2,507	33.5	.100	19,955	9.2	.187
22-a	-2	.2	0	2	.2	0	75	.1	.001
22-b	-1	-.1	-.001	-8	-.1	0	-75	0	-.001
23-a	-124	-2.8	-.021	-247	-2.7	-.010	-1,777	-.6	-.017
23-b	124	2.8	.021	247	2.7	.010	1,782	.6	.016
24-a	-65	-1.5	-.011	-223	-8.1	-.010	-3,450	-3.9	-.037
24-b	65	1.5	.011	223	8.1	.010	3,460	3.9	.037
25-a	-16	-.4	-.003	-56	-2.0	-.003	-3,102	-6.2	-.038
25-b	16	.4	.003	56	2.0	.003	3,111	6.2	.037
26-a	-5	-.1	-.001	-19	-.7	.000	-1,035	-2.1	-.013
26-b	5	.1	.001	19	.7	.001	1,036	2.1	.013

TABLE IV.- ORBITAL-ALTITUDE VARIATION DUE TO EACH ERROR SOURCE AT RANGE-ANGLE INCREMENTS FOR 300-NAUTICAL-MILE NOMINAL CIRCULAR ORBIT

[The case numbers refer to the error sources of table I; a and b are the +2σ and -2σ error values, respectively]

Case	Δh, ft	ΔV, ft/sec	Δγ, deg	Δh, nautical miles, for -											
				$\phi = 0°$	$\phi = 30°$	$\phi = 60°$	$\phi = 90°$	$\phi = 120°$	$\phi = 150°$	$\phi = 180°$	$\phi = 210°$	$\phi = 240°$	$\phi = 270°$	$\phi = 300°$	$\phi = 330°$
	h_{nom} = 1,822,830	V_{nom} = 24,875.92	γ_{nom} = 0.0	h_{nom} = 300 nautical miles											
1-a	33,183	6.2	0.181	5.46	12.36	19.40	24.68	26.76	25.07	20.09	13.16	6.15	3.334	-1.12	0.554
1-b	-33,710	-7.0	-.183	-5.55	-12.53	-19.65	-25.01	-27.22	-25.70	-20.84	-13.92	-6.77	-1.31	.959	-.598
2-a	30,223	35.5	.213	4.97	14.06	24.97	34.78	40.81	41.40	36.39	27.17	16.25	6.56	.666	.386
2-b	-29,895	-34.9	-.212	-4.92	-13.87	-24.47	-33.87	-39.61	-40.21	-35.54	-26.77	-16.19	-6.63	-.713	-.382
3-a	25,243	48.3	.206	4.15	13.41	25.25	36.54	44.20	46.12	41.75	32.32	20.42	9.25	1.77	-.090
3-b	-24,563	-47.2	-.203	-4.04	-13.08	-24.48	-35.19	-42.32	-44.20	-40.21	-31.40	-20.07	-9.21	-1.79	.108
4-a	275	33.3	.007	.045	1.63	5.48	10.59	15.58	19.11	20.24	18.64	14.76	9.64	4.66	1.15
4-b	217	-32.3	-.004	.036	-1.40	-5.03	-9.89	-14.65	-18.06	-19.82	-17.62	-14.25	-9.39	-4.59	-1.14
5-a	4,449	27.3	-.028	.732	-1.19	-4.59	-8.55	-12.02	-14.07	-14.15	-12.27	-8.90	-4.95	-1.44	.641
5-b	-7,361	-28.9	.017	-1.21	.331	3.46	7.34	10.94	13.29	13.79	12.20	9.06	5.17	1.58	-.757
6-a	8,589	-14.1	.025	1.41	1.84	1.40	.206	-1.41	-3.03	-4.21	-4.63	-4.20	-3.01	-1.39	.230
6-b	-9,623	13.4	-.029	-1.58	-2.21	-2.03	-1.07	.400	1.99	3.27	3.91	3.72	2.77	1.29	-.300
7-a	9,091	-10.0	.037	1.50	2.49	2.81	2.37	1.30	-.129	-1.52	-2.52	-2.84	-2.41	-1.34	.098
7-b	-9,477	12.7	-.035	-1.56	-2.41	-2.45	-1.61	-.181	1.49	2.94	3.60	3.32	3.01	1.57	-.104
8-a	609	2.6	.018	.100	.806	1.56	2.16	2.44	2.33	1.86	1.16	.407	-.192	-.476	-.369
8-b	-190	-.09	-.017	-.031	-.583	-1.00	-1.18	-1.06	-.684	-.149	.403	.823	.999	.883	.500
9-a	13,933	-7.9	.087	2.29	5.78	9.58	12.69	14.27	13.89	11.65	8.16	4.35	1.26	-.313	.066
9-b	-15,201	11.6	-.095	-2.50	-6.41	-10.86	-14.35	-16.79	-16.72	-14.45	-10.58	-6.13	-2.30	-.121	-.135
10-a	5,729	16.4	.058	.943	3.63	7.17	10.63	13.06	13.83	12.72	10.03	6.48	3.23	.598	-.164
10-b	-5,727	-18.2	-.059	-.942	-3.72	-7.46	-11.16	-13.83	-14.77	-13.74	-11.00	-7.27	-3.56	-.749	.110
11-a	3,619	18.7	.048	.596	3.00	6.40	9.96	12.66	13.79	13.05	10.64	7.21	3.68	.967	-.139
11-b	-233	-12.8	-.020	-.038	-1.21	-3.11	-5.22	-6.96	-7.92	-7.79	-6.63	-4.74	-2.62	-.859	.038
12-a	-4,990	29.6	-.036	-.621	-.916	1.17	4.59	9.25	13.07	15.57	15.48	13.38	9.63	5.26	1.44
12-b	5,487	-30.5	.039	.973	1.05	-1.06	-4.86	-9.41	-13.23	-15.58	-15.73	-13.60	-9.89	-5.43	-1.47
13-a	209	-.5	-.001	.034	.073	.092	.085	.056	.011	-.038	-.070	-.091	-.069	-.039	-.014
13-b	1,213	.6	-.007	.200	.488	.797	1.04	1.16	1.12	.951	.643	.334	.067	-.132	.210
14-a	15,193	-34.3	.093	2.50	4.46	3.82	.706	-4.01	-9.05	-13.08	-15.04	-14.40	-11.33	-6.64	-1.52
14-b	-14,800	31.3	-.090	-2.44	-4.44	-4.04	-1.36	2.90	7.61	11.51	13.54	13.15	10.45	6.15	1.44
15-a	10,052	-39.1	-.008	-1.65	.034	-3.56	-8.96	-13.89	-17.36	-18.44	-16.85	-13.02	-7.94	-2.96	.156
15-b	-11,239	37.2	-.001	-1.85	-.625	2.77	7.42	12.11	15.56	16.85	15.62	12.20	7.51	2.85	-.582
16-a	26,615	-52.6	.079	4.38	5.41	3.07	-1.99	-8.39	-14.40	-18.45	-19.47	-17.19	-12.20	-5.81	.267
16-b	-19,787	42.5	-.053	-3.26	-3.72	-1.52	2.76	7.99	12.78	15.83	16.3	14.09	9.78	4.55	-.247
17-a	29,891	-43.6	.125	4.92	7.91	7.88	4.84	-.378	-6.36	-11.10	-14.45	-14.44	-11.47	-6.77	-.381
17-b	-17,321	37.1	-.059	-2.85	-3.68	-2.08	1.53	6.19	10.66	13.73	14.58	12.97	9.33	4.05	.138
18-a	-4,552	-15.9	-.033	-.749	-2.58	-5.39	-8.44	-10.69	-12.11	-11.75	-9.97	-7.17	-4.12	-1.04	-.434
18-b	17,383	-18.7	.059	2.86	4.43	4.83	3.97	2.04	-.561	-2.86	-4.27	-4.63	-3.77	-1.88	.557
19-a	7,895	-47.8	1.32	1.30	43.10	69.99	75.69	53.07	14.59	-30.42	-69.84	-93.97	-97.32	-79.09	-46.34
19-b	-9,859	20.1	-1.33	-1.62	-44.22	-74.11	-84.36	-72.81	-41.96	.773	45.13	75.15	90.98	76.61	42.66
20-a	635	-1.4	.060	.105	2.02	3.35	3.72	3.04	1.49	-.102	-2.42	-3.74	-4.11	-3.44	-1.89
20-b	-144	.8	-.057	-.024	-1.84	-3.11	-3.50	-2.89	-1.47	.407	2.25	3.51	3.90	3.29	1.86
21-a	-21,773	-9.5	-.125	-3.58	-8.50	-13.81	-18.07	-20.18	-19.59	-15.44	-11.56	-6.25	-1.93	.225	-.381
21-b	22,225	4.4	.127	3.66	8.47	13.33	16.93	18.30	17.07	13.07	8.75	3.90	.325	-1.04	.185
22-a	330	.1	-.002	.054	.131	.210	.271	.296	.280	.227	.150	.071	.010	-.016	.001
22-b	164	0	-.001	.027	.074	.116	.141	.143	.121	[illegible]	.034	-.008	-.033	-.039	-.011
23-a	-1,707	-.4	-.009	-.281	-.640	-1.01	-1.30	-1.42	-1.34	-1.09	-.737	-.365	-.060	.043	-.031
23-b	2,202	.3	.012	.362	.816	1.27	1.61	1.73	1.62	[illegible]	.834	.378	.042	-.085	.033
24-a	-3,610	-3.5	-.024	-.594	-1.60	-2.78	-3.81	-4.42	-4.46	-3.90	-2.90	-1.72	-.686	-.066	-.052
24-b	4,111	3.3	.027	.677	1.79	3.06	4.13	4.72	4.68	4.01	2.90	1.63	.561	-.032	.008
25-a	-3,281	-5.8	-.026	-.540	-1.69	-3.15	-4.51	-5.42	-5.63	-5.10	-3.95	-2.50	-1.13	-.213	.003
25-b	3,782	5.6	.029	.622	1.89	3.43	4.84	5.73	5.67	[illegible]	3.96	2.41	1.01	.114	-.027
26-a	-945	-21.6	-.011	-.155	-1.40	-4.09	-7.50	-10.71	-12.87	-13.42	-12.20	-9.53	-6.12	-2.59	-.702
26-b	1,437	21.7	.014	.237	1.60	4.41	7.91	11.18	13.33	13.78	12.47	9.60	6.09	2.82	.684
$\sqrt{\Sigma(+\Delta h)^2} = (\Delta h)_{+2\sigma}$				12.56	51.72	84.41	98.32	94.51	84.20	77.93	78.78	90.91	94.25	77.95	43.01
$\sqrt{\Sigma(-\Delta h)^2} = (\Delta h)_{-2\sigma}$				-11.42	-51.82	-87.30	-106.24	-106.57	-92.97	-84.54	-96.46	-105.99	-101.98	-80.43	-43.50
$h + (\Delta h)_{+2\sigma}$				312.56	351.72	384.41	398.32	394.51	384.20	377.93	378.78	390.91	394.25	377.95	343.01
$h - (\Delta h)_{-2\sigma}$				288.58	248.18	212.70	193.76	193.43	207.03	215.46	203.54	194.01	198.02	219.57	256.50

TABLE V.- ORBITAL-ALTITUDE VARIATION DUE TO EACH ERROR SOURCE AT RANGE-ANGLE INCREMENTS FOR 300-NAUTICAL-MILE NOMINAL INJECTION ALTITUDE AND $V_i/V_c = 1.00$

[The case numbers refer to the error sources of table I; a and b are the $+2\sigma$ and -2σ error values, respectively]

Case	Δh, ft	ΔV, ft/sec	$\Delta\gamma$, deg	Δh, nautical miles, for -											
				ϕ = 0°	ϕ = 30°	ϕ = 60°	ϕ = 90°	ϕ = 120°	ϕ = 150°	ϕ = 180°	ϕ = 210°	ϕ = 240°	ϕ = 270°	ϕ = 300°	ϕ = 330°
	h_{nom} = 1,822,830	V_{nom} = 25,373.44	γ_{nom} = 0.0	h_{nom} = 300	h_{nom} = 319.58	h_{nom} = 374.13	h_{nom} = 451.26	h_{nom} = 531.57	h_{nom} = 592.49	h_{nom} = 615.26	h_{nom} = 592.49	h_{nom} = 531.57	h_{nom} = 451.26	h_{nom} = 374.13	h_{nom} = 319.58
1-a	33,183	6.2	0.181	5.46	12.42	19.90	26.12	29.25	27.98	22.37	14.16	6.06	0.44	-1.45	0.46
1-b	-33,710	-7.0	-.183	-5.55	-12.58	-20.16	-26.50	-29.78	-28.68	-23.19	-14.97	-6.68	-.81	1.28	-.54
2-a	30,223	35.5	.213	4.97	14.05	25.38	36.44	44.16	45.81	40.36	29.43	16.70	6.10	.22	-.03
2-b	-29,895	-34.9	-.212	-4.92	-13.90	-24.98	-35.69	-43.12	-44.72	-39.52	-28.97	-16.54	-6.06	-.20	.06
3-a	25,243	48.3	.206	4.15	13.38	25.62	38.19	47.71	50.91	46.24	35.03	21.10	8.81	1.27	-.24
3-b	-24,563	-47.2	-.203	-4.04	-13.38	-24.94	-36.99	-46.05	-49.10	-44.71	-34.06	-20.65	-8.67	-1.22	.28
4-a	275	33.3	.007	.05	1.56	5.38	10.80	16.53	20.90	20.39	15.66	9.82	4.56	1.10	-1.07
4-b	217	-32.3	-.004	.04	-1.33	-4.95	-10.11	-15.60	-19.82	-21.32	-19.53	-15.12	-9.56	-4.48	2.80
5-a	4,449	27.3	-.028	.73	.99	3.48	7.91	13.26	18.04	20.66	20.20	16.87	11.90	6.79	-5.05
5-b	-7,361	-28.9	.017	-1.21	-1.92	-5.10	-10.16	-15.99	-20.82	-23.16	-22.12	-18.12	-12.56	-7.10	.24
6-a	8,589	-14.1	.025	1.41	1.89	1.54	.39	-1.34	-3.22	-4.63	-5.11	-4.53	-3.14	-1.40	-.33
6-b	-9,623	13.4	-.029	-1.58	-2.24	-2.14	-1.25	.29	2.08	3.59	4.29	3.99	2.85	1.27	-.13
7-a	9,091	-10.0	.037	1.50	2.54	2.97	2.66	1.58	-.01	-1.66	-2.81	-3.13	-2.57	-1.38	.09
7-b	-9,477	12.7	-.035	-1.56	-2.44	-2.56	-1.83	-.35	1.53	3.23	4.19	4.12	3.12	1.56	-.13
8-a	609	2.6	.018	.10	.81	1.59	2.28	2.66	2.59	2.06	1.23	.37	-.27	-.52	-.38
8-b	-190	-.1	-.017	-.03	-.60	-1.06	-1.29	-1.21	-.80	-.17	.49	.95	1.11	.94	.52
9-a	13,935	-7.9	.087	2.29	5.17	7.43	8.48	7.89	5.66	2.57	-.93	-3.19	-3.81	-2.80	-.57
9-b	-15,201	11.6	-.095	-2.50	-5.53	-7.67	-8.56	-7.23	-4.42	-.68	2.78	4.87	5.06	3.49	.74
10-a	5,729	16.4	.058	.94	3.61	7.27	11.10	14.11	15.28	14.09	10.87	6.70	2.89	.44	-.21
10-b	-5,727	-18.2	-.059	-.94	-3.71	-7.58	-11.69	-14.97	-16.36	-15.25	-11.93	-7.52	-3.40	-.66	.18
11-a	3,619	18.7	.048	.60	2.98	6.48	10.37	13.63	15.21	14.46	11.56	7.50	3.58	.84	-.19
11-b	-233	-12.8	-.020	-.04	-1.20	-3.12	-5.41	-7.49	-8.72	-8.63	-7.23	-4.96	-2.60	-.77	.12
12-a	-4,990	29.6	-.036	-.82	-.99	.99	4.82	9.67	14.23	16.99	16.99	14.31	9.93	5.24	1.39
12-b	5,487	-30.5	.039	.90	1.14	-.84	-4.74	-9.70	-14.38	-17.25	-17.33	-14.66	-10.24	-5.43	-1.44
13-a	209	-.3	-.001	.03	-.01	-.05	-.09	-.12	-.12	-.09	-.04	.01	.05	.07	.06
13-b	1,213	.6	-.007	.20	.02	-.03	.09	.35	.70	1.03	1.23	1.25	1.06	.80	.48
14-a	15,193	-34.3	.093	2.50	4.59	4.20	1.24	-3.80	-9.63	-14.44	-16.64	-15.60	-11.87	-6.72	-1.55
14-b	-14,800	31.3	-.090	-2.44	-4.53	-4.38	-1.84	2.69	8.09	12.69	14.96	14.22	10.92	6.21	1.41
15-a	10,052	-39.1	-.008	1.65	.11	-3.72	-9.10	-14.75	-19.01	-20.42	-18.43	-13.76	-7.99	-2.79	.64
15-b	-11,239	37.2	-.001	-1.85	-.71	2.60	7.47	12.77	16.96	18.60	17.06	12.92	7.63	2.72	-.64
16-a	26,615	-52.6	.079	4.38	5.55	3.52	-1.49	-8.45	-15.48	-20.36	-21.42	-18.45	-12.61	-5.76	.34
16-b	-19,787	42.5	-.053	-3.26	-3.82	-1.81	2.50	8.22	13.81	17.45	17.87	15.04	10.03	4.44	-.33
17-a	29,891	-43.6	.125	4.92	8.03	8.38	5.64	.22	-6.55	-12.62	-15.97	-15.63	-11.97	-6.31	-.22
17-b	-17,321	37.1	-.059	-2.89	-3.76	-2.35	1.24	6.30	11.49	15.14	16.01	13.88	9.62	4.65	.13
18-a	-4,552	-15.9	-.033	-.75	-2.55	-5.42	-8.75	-11.71	-13.36	-13.07	-10.88	-7.54	-4.12	-1.55	-.37
18-b	17,383	-18.7	.059	2.86	4.48	5.06	4.38	2.49	-.20	-2.88	-4.67	-5.02	-3.95	-1.88	.98
19-a	7,895	-47.8	1.32	1.30	43.41	72.85	80.78	62.36	20.78	-31.62	-77.80	-103.90	-104.41	-81.91	-45.67
19-b	-9,859	20.1	-1.33	-1.62	-44.70	-77.14	-91.10	-81.11	-46.98	3.22	53.99	88.59	97.03	79.57	43.27
20-a	635	-1.4	.060	.11	2.05	3.49	4.04	3.45	1.77	-.55	-2.78	-4.16	-4.44	-3.57	-1.91
20-b	-144	.8	-.057	-.24	-1.88	-3.26	-3.82	-3.30	-1.74	.45	2.56	3.96	4.23	3.44	1.69
21-a	-21,773	-9.5	-.125	-3.58	-8.55	-14.16	-19.13	-22.06	-21.84	-18.29	-12.46	-6.26	-1.57	.49	-.31
21-b	22,225	4.4	.127	3.66	8.52	13.68	17.94	20.03	19.06	15.11	9.39	3.79	-.09	-1.28	.13
22-a	330	.1	-.002	.05	0	-.02	.00	.07	.16	.25	.31	.32	.29	.22	.13
22-b	164	0	-.001	.27	-.00	-.02	-.02	.01	.04	.09	.12	.13	.13	.10	.69
23-a	-1,707	-.4	-.009	-.28	-.63	-1.02	-1.35	-1.53	-1.49	-1.22	-.81	-.39	-.08	.04	-.04
23-b	2,202	.3	.012	.36	.82	1.30	1.70	1.89	1.80	1.43	.89	.37	.01	-.11	.03
24-a	-3,610	-3.5	-.024	-.59	-1.60	-2.83	-4.01	-4.81	-4.95	-4.54	-3.14	-1.76	-.63	-.01	-.02
24-b	4,111	3.3	.027	.68	1.79	3.10	4.33	5.12	5.19	4.46	3.14	1.68	.51	-.07	.00
25-a	-3,281	-5.8	-.026	-.54	-1.69	-3.20	-4.73	-5.87	-6.24	-5.66	-4.26	-2.58	-1.07	-.15	.02
25-b	3,782	5.6	.029	.62	1.88	3.47	5.05	6.19	6.50	5.80	4.30	2.50	.96	.06	-.04
26-a	-945	-21.6	-.011	-.16	-1.37	-4.07	-7.72	-11.45	-14.15	-14.88	-13.34	-10.08	-6.19	-2.78	-.65
26-b	1,437	21.7	.014	.24	1.56	4.38	8.13	11.92	14.61	15.25	13.56	10.15	6.16	2.73	.64
$\sqrt{\Sigma(+\Delta h)^2} = (\Delta h)_{+2\sigma}$				12.68	51.98	87.09	105.25	104.29	93.32	86.56	89.54	102.15	101.79	80.76	43.30
$\sqrt{\Sigma(-\Delta h)^2} = (\Delta h)_{-2\sigma}$				11.42	52.20	90.06	112.96	116.20	102.52	93.26	107.22	116.94	109.56	83.53	45.90
$h + (\Delta h)_{+2\sigma}$				312.68	371.56	461.22	556.51	635.66	689.81	701.82	682.63	633.72	553.05	454.89	362.88
$h - (\Delta h)_{-2\sigma}$				288.58	267.38	284.07	338.50	415.57	489.97	522.00	489.28	414.63	341.70	290.60	275.58